**TOPICAL REVIEW**

# Printed and organic diodes: devices, circuits and applications

View the article online for updates and enhancements.

# Flexible and Printed Electronics

# Printed and organic diodes: devices, circuits and applications

Thomas M Kraft[1] , Paul R Berger[1,2] and Donald Lupo[1]

[1] Tampere University of Technology, Electronics and Communications Engineering, PO Box 692, FI-33101 Tampere, Finland
[2] Department of Electrical and Computer Engineering, The Ohio State University, Columbus, OH 43210, United States of America

E-mail: donald.lupo@tut.fi

## Abstract

We review the history and current state of the art of diodes fabricated with organic semiconductors and other printable materials. In particular, we look at the integration of printed diodes into circuits and systems for applications, with particular emphasis on rectification, energy harvesting, and negative differential resistance (e.g. tunnel diodes). An overview of solution processed and printable organic and inorganic materials utilised in diodes is provided with an in depth analysis of their physics of operation. Furthermore, it is explained how the diverse array in which printed diodes can be implemented demonstrates their potential in the printed electronics industry.

## 1. Introduction

The foreseen advantages of organic semiconductor materials rely on the possibility to fabricate electronic components and circuits using cost-effective manufacturing processes. A large number of devices have been demonstrated, such as organic field-effect transistors (OFET) [1–14], photovoltaics (OPV) [15–20] and light-emitting diodes (OLED) [21]. These topics have been extensively reported in the literature. There has been less emphasis on purely electronic diodes, but these are important not only for a better understanding of the device physics of OPV and OLED devices [22, 23], but also for their use as components in a variety of circuits.

In this review we will focus on rectifying diodes and will not address OPV [19, 24–27] or OLED [28, 29] in any detail; for these topics the reader is recommended to consult some of the excellent reviews which have appeared recently. In section 2 we discuss the basic architectures for organic and printed diodes, specifically Schottky, metal–insulator–metal (MIM) and doped p–n junction devices and review the development in understanding of how these devices work. In section 3 we review the classes of materials that have been used, including both evaporated and solution processed organic semiconductors as well as solution processed inorganic materials. In section 4 we review the progress in increasing the switching speed of organic and printed diodes and investigate the factors currently limiting high-speed operation. This section also includes the achievements in integration of organic and printed diodes into
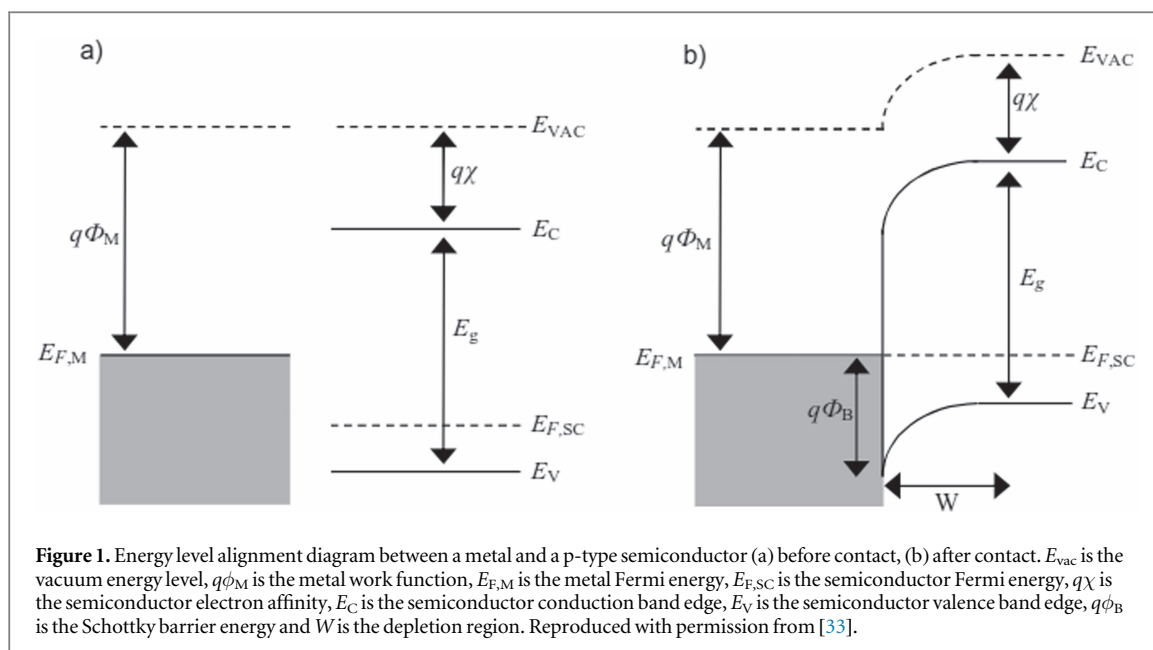
functional circuits for applications such as rectification, RF energy harvesting and thin-film-diode (TFD) display backplanes. In section 5 we review a recent special case of solution processed diodes, namely tunnel diodes.

In order to adequately cover novel progress in the field but keep the scope of this review manageable, we have chosen to discuss diodes that are based on organic semiconductors and/or are fabricated using solution processing. For example, organic diodes made by vacuum evaporation are included, as are metal oxide devices fabricated from solution, but we do not include metal oxide devices made using the vacuum processes that are seeing substantial commercialisation, e.g. in TFT display backplanes [30, 31].

## 2. Organic diode architectures

The diode is a quintessential component used in electronics to control the unidirectional flow of current. A key component of a diode is a junction that allows current to flow in one direction but not in another. The most common diodes in conventional electronics are based on p–n homo- or heterojunctions; the physics of such diodes is well described and part of a basic education in solid state physics [32], therefore will not be described further here.

Another common type of diode in the conventional electronic industry is a Schottky diode, which consists of a layer of p or n type semiconductor situated between two contacts, one of which is Ohmic and

**Figure 1.** Energy level alignment diagram between a metal and a p-type semiconductor (a) before contact, (b) after contact. $E_{vac}$ is the vacuum energy level, $q\phi_M$ is the metal work function, $E_{F,M}$ is the metal Fermi energy, $E_{F,SC}$ is the semiconductor Fermi energy, $q\chi$ is the semiconductor electron affinity, $E_C$ is the semiconductor conduction band edge, $E_V$ is the semiconductor valence band edge, $q\phi_B$ is the Schottky barrier energy and $W$ is the depletion region. Reproduced with permission from [33].

one of which blocks charge injection in one bias but not in the other [32]. Figure 1 below shows a sketch of a Schottky contact between metal and p type semiconductor [33]. On the left side of the figure, the metal and semiconductor are isolated from each other. When they are brought together in equilibrium, the Fermi levels align. As long as the work function of the metal and the Fermi level of the semiconductor are not the same, this alignment includes movement of charges in the region close to the interface and leads to band bending. In the case of a metal work function smaller than the distance from the semiconductor Fermi level to the vacuum, this leads to a depletion region close to the interface. Under forward bias holes can move more or less unhindered from the semiconductor into the metal, while under reverse bias there is a significant barrier to hole injection from the metal, leading to rectifying behaviour of the diode.

Many solution processed organic diodes are single layer devices due to the difficulty of multilayer solution coating or printing, and are based on a semiconductor with primarily electron or hole conduction properties. For this reason, the Schottky model is commonly used in describing solution processed diodes. However, at least for organic diodes this model may be questionable. This begins with the differences in energy level structure and charge transport in organic semiconductors [34]. Energy states in organic semiconductors are far less localised than in conventional semiconductors and it is common to use the terms 'highest occupied molecular orbital' (HOMO) and 'lowest unoccupied molecular orbital' (LUMO) instead of valence and conduction band, respectively. Charge transport is also not ballistic but dominated by hopping from one semi-localised energy state to another. In addition, most of the time (we will discuss doped semiconductor devices below) organic semiconductors are used in an undoped, quasi-intrinsic

state, and the terms 'p type' and 'n type' refer to relative charge carrier mobility and not to carrier concentration as in conventional semiconductors. Using typical estimates of intrinsic charge carrier densities in organic materials [33] a simple Schottky model would predict a depletion region of several $\mu$m, compared to typical diode thicknesses from a few 10 s to a few 100 s of nm.

Therefore it may be more suitable to speak of most organic diodes as MIM diodes. At equilibrium, there is no band bending at the Schottky contact and some band bending at the Ohmic contact due to hole injection [35]. In forward bias (figure 2(a)) the hole is easily injected from the anode ($x = 0$) and extracted by the cathode ($x = L$). In reverse bias, shown in figure 2(b), the hole would have to be injected over the significant Schottky barrier from the cathode into the semiconductor and very little current flows.

Blom *et al* have studied the physics of single-carrier organic MIM diodes in some detail, to a large extent as a means for better understanding of OLEDs and OPV devices [35–37]. As seen in figure 2 above, the bands in the intrinsic semiconductor are tilted at equilibrium with a built-in voltage equal to the difference in electrode work functions, due to the alignment of the Fermi levels of the electrodes. If one contact is Ohmic and one is rectifying, there will be a small or no barrier for injection of charge carriers (in organics, usually holes) in forward bias. The Schottky contact is chosen so that the barrier both for electron injection in forward bias and hole injection in reverse bias is too large for significant current to flow. In the common operational region of organic MIM diodes, drift current dominates, and a net (positive) space charge is built up within the device, which leads to an electric field within the semiconductor [35]. This space charge limits the current that can flow, i.e. the I–V behaviour is dominated by space charge limited current (SCLC).
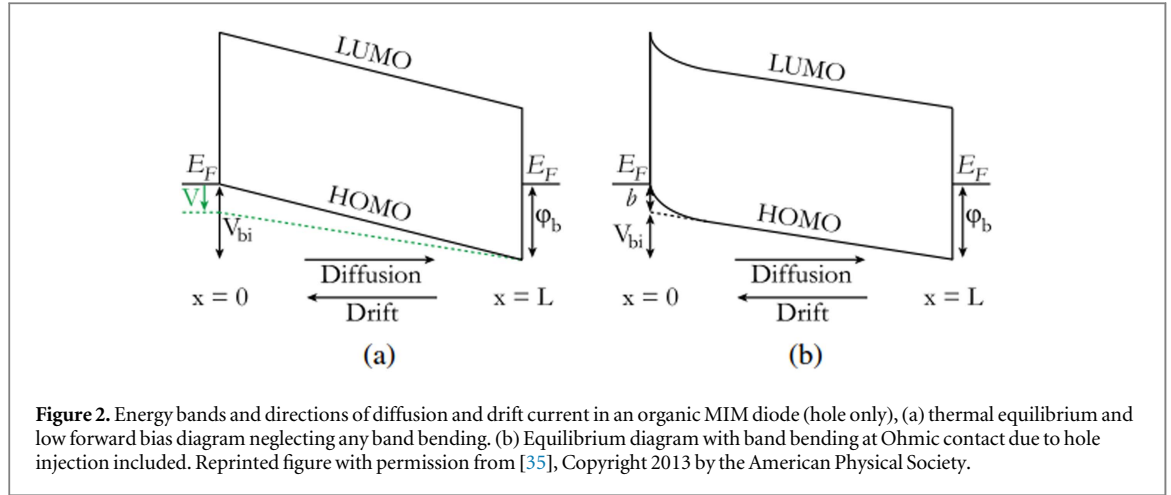
**Figure 2.** Energy bands and directions of diffusion and drift current in an organic MIM diode (hole only), (a) thermal equilibrium and low forward bias diagram neglecting any band bending. (b) Equilibrium diagram with band bending at Ohmic contact due to hole injection included. Reprinted figure with permission from [35], Copyright 2013 by the American Physical Society.

In the SCLC limit, the current is given by the expression of Mott and Gurney [38]:

$$J = \frac{9}{8}\varepsilon\mu\frac{(V - V_{bi})^2}{L^3} \, , \tag{1}$$

where $V_{bi}$ is the built-in voltage defined by the electrode work function difference. The SCLC limit only applies when the applied voltage is larger than the built-in voltage. Below this, the electric field is opposite in sign to the applied voltage, and current is dominated by diffusion due to the hole gradient, which is much larger than the negative drift current from the electric field. In the past, the Shockley diode equation has been applied to describe this region of operation:

$$J = J_0\left[\exp\left(\frac{qV}{\eta kT}\right) - 1\right], \tag{2}$$

where $J_0$ is an empirical analogue to the reverse saturation current in ideal p–n junction diodes and $\eta$ is the ideality factor. However, this model was developed to apply to p–n junction diodes, where the ideality factor is related to recombination of injected minority carriers and may not be suitable for MIM single-carrier diodes.

De Bruyn *et al* studied the current–voltage characteristics of hole-only MIM organic diodes below SCLC [35] in detail based on Schottky's model of diffusion current at metal–semiconductor interfaces [39]. The model needs to be modified from the original theory, which described a contact between metal and doped semiconductor and diffusion of majority carriers to match Fermi levels. In MIM diodes, there are no dopants to induce band bending at the Schottky contact, so that the treatment of the diffusion current needs to consider the entire semiconductor thickness. Within this model, they found the following expression for the current density in the region below the built-in voltage:

$$J_P = \frac{q\mu_p N_v(\varphi_b - V)\left[\exp\left(\frac{qV}{kT}\right) - 1\right]}{L\left[\exp\left(\frac{q\varphi_b}{kT}\right) - \exp\left(\frac{qV}{kT}\right)\right]}. \tag{3}$$
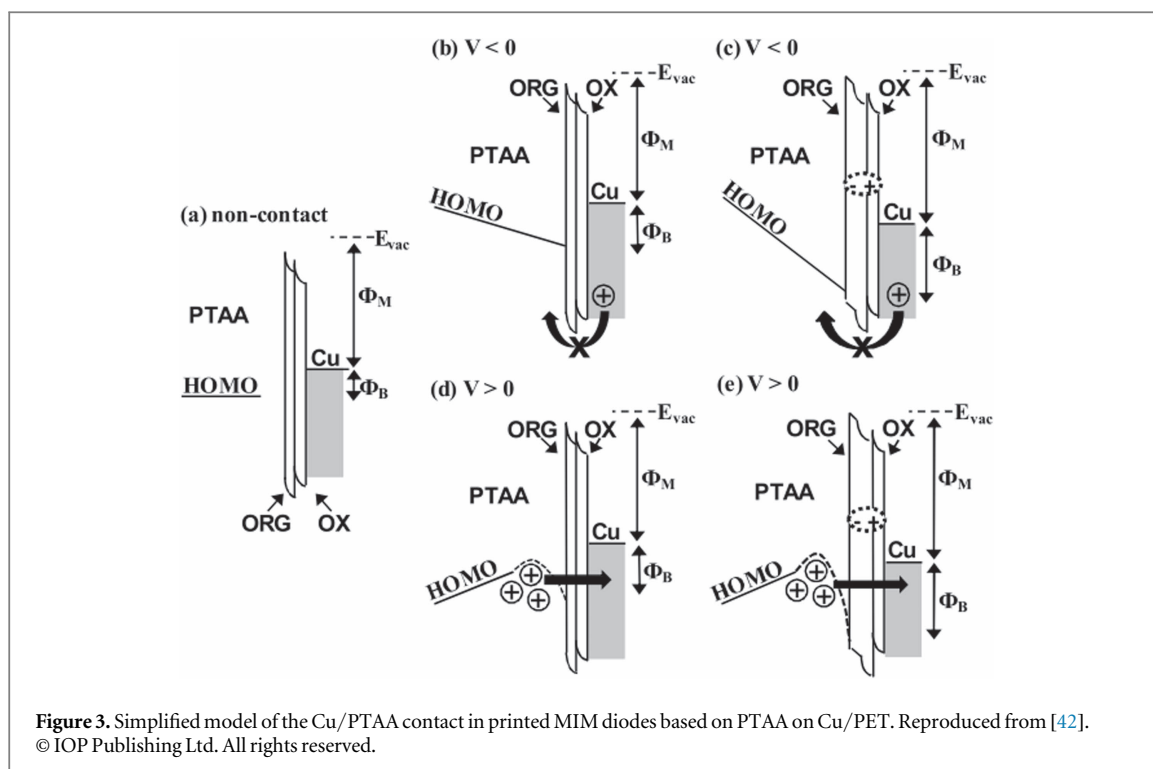
Almost the same equation was derived earlier by Nguyen *et al* [40] in their analysis of two-carrier OLED devices. However, implicit in this equation is the assumption that the built-in voltage is equal to the difference in electrode work functions. This is not entirely accurate because of hole injection at the Ohmic contact (see figure 2(b)) where there is some hole injection from the electrode leading to a small accumulation region and band bending in the semiconductor, which reduces the built-in voltage. De Bruyn *et al* approximated this by maintaining a straight line band diagram with an added energy shift *b* characterising the reduction in built-in voltage. As a result, equation (3) is simply modified by replacing $\phi_b$ by $\phi_b$–*b* for $V_{bi}$ and describes the *I–V* behaviour up to $\phi_b$–*b*, above which equation (1) holds. They found also that this modification to the Schottky formalism explained the typical non-ideality factor of 1.2 seen in the sub-SCLS region of organic MIM diodes.

Wetzelaer and Blom [37] later also considered the case of a symmetrical (non-rectifying) hole only MIM device with two Ohmic contacts. Due to the band bending and diffusion of charge described above, an Ohmic current is seen even if the semiconductor is completely free of inherent charge carriers, and the current density below the built-in voltage is given by

$$J = 4\pi^2\frac{kT}{q}\varepsilon\mu\frac{V}{L^3}. \tag{4}$$

They recommended using the *I–V* characteristics in this region as a method to determine the charge carrier mobility of the material, as changes in mobility due to charge carrier density are not yet significant.

MIM diodes based on polymers represent a very simple structure, which is easily fabricated by large-area, high volume printing technologies, as high lateral resolution is not needed. However, printing a diode in laboratory ambient air is very different than spin

**Figure 3.** Simplified model of the Cu/PTAA contact in printed MIM diodes based on PTAA on Cu/PET. Reproduced from [42].

coating organic materials in a glove box and evaporating clean metal contacts. Since the nature of the metal–semiconductor contact is crucial for performance of the devices, it is not surprising that printed diodes may show behaviour that a simple application of literature values for semiconductor energy levels and electrode work functions would not predict. Lilja *et al* [41, 42] fabricated MIM diodes in a particularly simple process, starting with wet-etched patterned Cu on PET as substrate and gravure printing the air-stable amorphous organic hole transporting semiconductor poly (triarylamine) (PTAA) and a top electrode of a silver-flake ink. Based on literature values of the work functions of Ag and Cu of 4.3 and 4.7 eV, respectively, and a HOMO level of PTAA of 5.1 eV, two Schottky contacts with different energy barriers could be expected. However, *I–V* measurements showed SCLC at low voltages, rectification ratios up to $10^5$, and also that Ag was clearly the anode and Cu the cathode. Furthermore, the rectification ratio varied between $10^5$ if the copper was sputter deposited before patterning and $10^3$ for thermally evaporated Cu, and the onset of SCLC was 0.2 V for evaporated and ca 2 V for sputtered copper. Kelvin probe measurements showed that the Ag was heavily oxidised and had an effective work function of ca 5.1 eV due to the large amount of $Ag_2O$ in the electrode. Impedance spectroscopy and XPS analysis of the Cu/PET layer shed more light on the Cu/PTAA interface; in both cases nm scale layers of Cu(I) oxide and organic material were found, but the layers were significantly thicker on the sputtered Cu/PET films. Based on this, it was proposed [42] that the double layer of two materials of different dielectric constant changes the effective energetics of the metal–

semiconductor interface, This causes Cu to act as an effective cathode and blocks hole injection in reverse bias. In forward bias, the build-up of charge at the interface generates a field that allows effective tunnelling of holes through the interlayer for collection by the Cu electrode (see figure 3).

An impressive example of the importance of interfaces in organic MIM diodes was reported by Cölle *et al* [43]. They made electron-only devices with a number of different polymers (even including insulating polystyrene) and the small molecule OLED material $Alq_3$. In about a third of the devices, multiple conductive states were observed leading to substantially different *I–V* curves. It was possible to switch between the state by applying suitable voltage pulses, so that the devices could be operated as non-volatile memory cells. The key to the memory effect was identified as the oxide layer between the organic and the aluminium electrode.

Most solution processed or printed diodes are based on vertical structures in order to be more printing compatible by reducing the demands on lateral resolution. A different and novel approach was reported by Anthopoulos *et al* [44–46] which they termed adhesion lithography. In this approach one metal is deposited, then coated with a self-adsorbed monolayer (SAM). Subsequently, a second metal which adheres poorly to the SAM is deposited. An adhesive tape is then applied to the substrate and peeled off; this removes the second metal from the area coated by the SAM and leaves the second metal elsewhere, with a ca 15 nm gap between the two metals. Using this technique and a solution processable ZnO semiconductor, they demonstrated fabrication of diodes operating at

up to 13.56 MHz. Printed metal oxide diodes have also been reported in vertical configurations, but we will discuss these in the section on switching and applications.

The diodes discussed above are all generally MIM diodes and best modelled accordingly; this accounts for the vast majority of organic and printed rectifying diodes. However, a p–n or p–i–n structure is also fundamentally possible in organics, and in particular Leo *et al* have reported extensively on this [47], especially for applications in OLEDs and OPV. They have also reported rectifying diodes based on such structures. As the conductivity of a semiconductor depends linearly on both the charge carrier mobility and charge carrier concentration, doping of organic semiconductors, which have significantly lower mobility than conventional crystalline semiconductors, can strongly reduce resistive losses and transit time in the diode. Furthermore, heavy doping can cause an Ohmic or quasi-Ohmic contact between many different electrode materials and the doped semiconductor due to the very narrow depletion layer at the contact. This has been proven to be useful in designing OLEDs that do not depend on highly oxidisable electrode materials such as Ca [47]. On the other hand, this approach is difficult to apply to solution processed or printed devices, so this technique has thus far largely been limited to devices prepared by vacuum evaporation.

Kleeman *et al* [48] applied the p–i–n structure to rectifying diodes, using a heterojunction stack of p-doped pentacene, intrinsic pentacene, and n-doped $C_{60}$. In addition to optimising the doping of the p and n layers, the thickness of the intrinsic layer, over which the main voltage drop in the device occurs, was optimised to find the best value to deliver large rectification (aided by a thicker layer) and shorter transit time (aided by a thinner layer). The same group also studied reverse-bias breakdown behaviour in such p–i–n diodes [49, 50] and found strong evidence that the reverse breakdown was due to Zener tunnelling between HOMO and LUMO of the p- and n-doped parts of the stack through a depletion layer defined primarily by the thickness of the intrinsic layer. The thickness dependence of breakdown voltage, coupled with a weak temperature dependence, was seen as strong evidence that the mechanism is tunnelling and not avalanche breakdown. Furthermore, the breakdown voltage could be tuned over a wide range, from ca $-6$ to $-18$ V by controlling both the order of deposition of the stack (n–i–p versus p–i–n) and the thickness of the intrinsic layer.

# 3. Semiconductor materials for diodes

In this section, we review both evaporated and solution processed organic semiconductors as well as solution processed inorganic materials used in diodes. Like other printed electronics, solution processed diodes have the potential to provide low cost and flexible alternatives to traditional diodes through printed fabrication. For example, the printing of a uniform polymer film can be performed in a number of different ways and these vary between those used for small scale tests in the lab and those used for high volume production. Common film forming techniques in the lab include spin coating, doctor blading and casting. For high volume processing it is possible to use coating techniques such as slot-die, gravure, knife-over-edge, off-set and spray coating [51]. In particular, printing techniques such as gravure, flexographic, screen, and inkjet can offer enhanced processing detail.

We have provided a review of some of the organic compounds and solution processed inorganic materials used in a variety of diodes. The materials and their processing conditions are summarised in table 1 with the organic materials structures illustrated in figure 4.
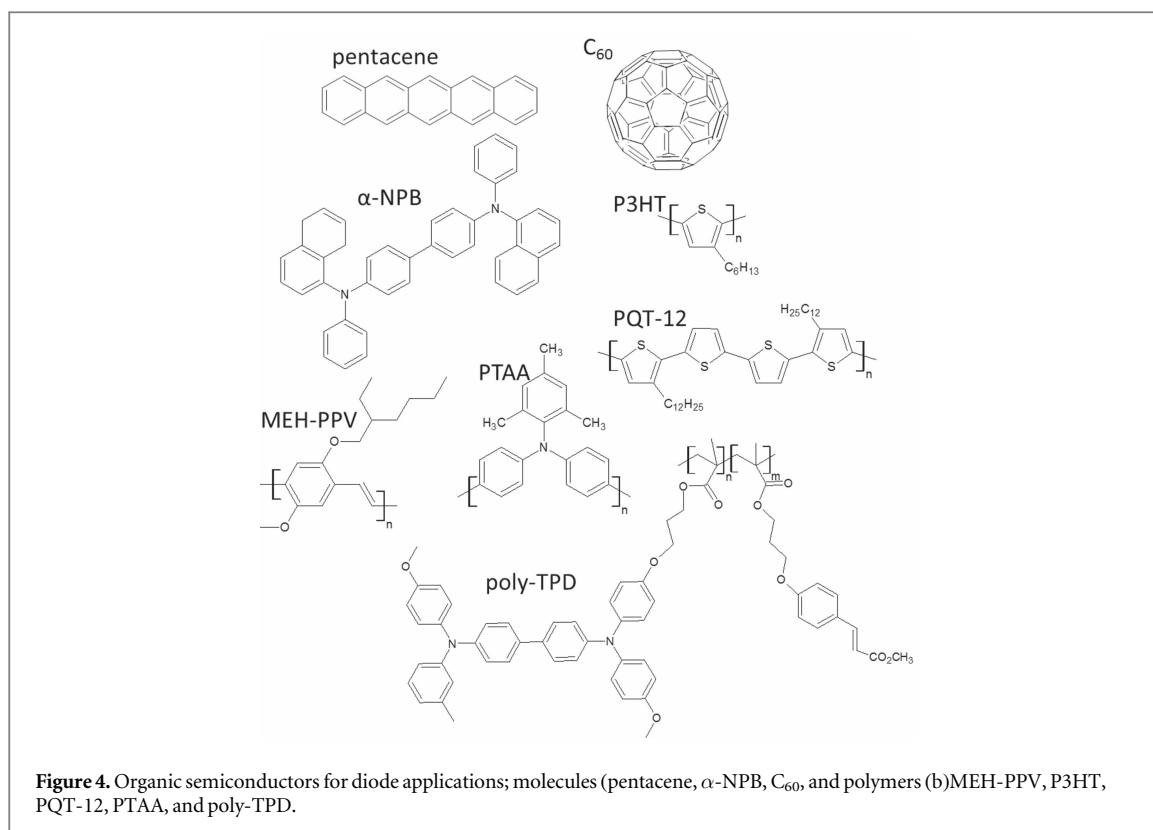
## 3.1. Organic materials for diodes

The unique electronic properties of conjugated organic compounds (molecules and polymers) allow them to be used for various electronic applications which include xerography, multi-element sensors, batteries, and organic electronics. Organic electronics can be fabricated with conjugated polymers or small molecules to fabricate a number of organic devices (i.e. FET, OLED, and OPVs), with their use in such devices enabled by the semiconducting electronic characteristic of the conjugated materials. A detailed description of conjugated organic molecules and polymers is readily found in recent literature and out of the context of this review.

With their inherent benefit for use in printing, conjugated polymers are of particular interest as they have enhanced solution processability over small molecules whose films are normally best achieved via vacuum processing (i.e. thermal sublimation). Semiconducting polymers have an unsaturated carbon based backbone with alternating single and double bonds [66]. Each carbon atom has one electron in a $p_z$ orbital that is not involved in the σ-bond. The $p_z$ orbitals between adjacent carbon atoms overlap to create a π-system. These overlapping $p_z$ orbitals form a delocalised π-electron cloud along the backbone of the polymer. The molecular energy levels of the π-band (HOMO) and the $π^*$-band (LUMO) provide a critical characteristic of the polymer. The energy difference between the HOMO and LUMO is known as the band gap, which is responsible for various characteristics including absorption, photoluminescence, and photoinduced charge transfer.

The electronic transport properties of a conjugated polymer are affected by several intrinsic and extrinsic properties. Intrinsic molecular level properties include ionisation potentials, electron affinity, coulomb correlations, and, as previously mentioned,

**Table 1.** Semiconducting materials and processing methods for organic and printed diodes.

| Semiconductor layer | Material type | Processing method | Example of application | Example of device architecture | Reference |
|---|---|---|---|---|---|
| 4,4′-bis[N-(1-naphthyl)-N-phenyl-amino]biphenyl [α-NPB] | Organic | Evaporated | Organic diode | Glass/ITO/α-NPB/Al | Haldi *et al* [52] |
| pentacene | Organic | Evaporated | 50 MHz rectifier organic diode | Glass/ITO/pentacene/Al | Steudel *et al* [53] Haldi *et al* [52] |
| Fullerene ($C_{60}$) | Organic | Evaporated | Organic diode | Glass/ITO/$C_{60}$/BCP/Al | Haldi *et al* [52] |
| $C_{60}$:polystyrene (95:5) | Organic | Spin coated | Schottky diode | Au/$C_{60}$:PS/Al | Semple *et al* [46] |
| poly(3-hexylthiophene) [P3HT] | Organic | Spin coated | Polymer diode | PC/IZO/(PEDOT:PSS)/P3HT/Al | Lin *et al* [54] |
| poly(3,3‴didodecylquaterthiophene) [PQT-12] | Organic | Spin coated | Polymer diode | PC/IZO/(PEDOT:PSS)/PQT-12/Al | Lin *et al* [54] |
| poly[2-methoxy-5-(2′-ethyl-hexyloxy)-1,4-phenyleneviny-lene] [MEH-PPV] | Organic | Spin coated | Tunnel diode (with $TiO_2$ layer) | Glass/ITO/$TiO_2$/MEH-PPV/Al | Yoon *et al* [55] |
| N,N′-bis(m-tolyl)-N,N′-diphenyl-1,1′-biphenyl-4, 4′-dia-mine [poly-TPD] | Organic | Spin coated | Polymer diode | Glass/ITO/poly-TDP /Al | Haldi *et al* [52] |
| poly[bis(4-phenyl)(2,4,6-trimethylphenyl)amine] a.k.a. poly (triarylamine) [PTAA] | Organic | Gravure printing | 13.56 and 10 MHz rectifying organic diodes | PET/Cu/PTAA/Ag and PET/Ag/$AgO_2$/PTAA/Cu | Li *et al* [56, 57] Lilja *et al* [58] Heljo *et al* [59–61] |
| Pentacene and ZnO | Hybrid | ZnO (dip-coated) pentacene (evaporated) | p–n junction diode | Glass/ITO/ZnO/pentacene/Au | Pal *et al* [62] |
| PQT-12 and ZnO | Hybrid | ZnO (dip-coated) pentacene (spin coated) | p–n junction diode | Glass/ITO/ZnO/PQt-12/Au | Sun *et al* [63] |
| P3HT and pentacene | Organic | P3HT (spin coated) pentacene (evaporated) | Schottky diode | Au/P3HT/pentacene/Al | Sun *et al* [63] |
| zinc oxide (ZnO) | Inorganic | Spin coated | Inorganic Schottky diode | Au/ZnO/Al | Semple *et al* [45, 46] |
| ZnO and $Ga_2O_3$ | Inorganic | Spin coated | Resonant tunnelling diode | Glass/Al/ZnO/ $Ga_2O_3$/ZnO/ $Ga_2O_3$/ZnO/Al | Labram *et al* [64] |
| Sb-doped Si and $NbSi_2$ microparticles in photoresist binder (SU8 2010) | Hybrid | Screen printing | 1.6 GHz diode | PET/Al/SU8:Sb-Si/SU8:$NbSi_2$/carbon paste/Ag | Sani *et al* [65] |

**Figure 4.** Organic semiconductors for diode applications; molecules (pentacene, $\alpha$-NPB, $C_{60}$, and polymers (b)MEH-PPV, P3HT, PQT-12, PTAA, and poly-TPD.

the HOMO–LUMO $\pi$-bands. The HOMO–LUMO band gap energy can also be described as the energy difference between the valence band and the conduction band ($E_G = E_V - E_C$). The energy associated with the valence band is equivalent to the ionisation potential and the energy of the conduction band is equivalent to the electron affinity. Extrinsic properties that have an effect on a polymer's transport properties include crystallinity, morphology, disorder, intermolecular interactions, and impurities. These properties can be controlled by carefully engineering the polymer's structure.

### 3.2. Inorganic materials for diodes

The use of solution processable inorganic semiconductors have not only provided a route for printable inorganic diodes but have found a use in numerous printed electronic devices, including OPVs [67–69], and FETs [70]. Solution processed inorganic films can be made with metal oxide semiconductors which can be prepared via a sol–gel precursor solution or dispersed in solvent. An example of a commonly used solgel, is for the formation of a thin zinc oxide (ZnO) film used in many device applications. The solgel can be deposited using spin coating and then annealed at 300 °C in air to form zinc oxide. An example of the ZnO sol–gel solution is comprised of zinc acetate ($Zn(O_2CCH_3)_2$) dissolved in 2-methoxyethanol:ethanolamine (96:4) [71]. The major disadvantage to the use of this particular solgel is the high annealing temperature necessary to form the oxide film. Another alternative was utilised by Semple *et al* in which a 0.25 M precursor solution was prepared by dissolving

zinc oxide hydrate in ammonium hydroxide (50% aqueous) [46]. This was then deposited by spin coating and annealed at 180 °C for 20 min to form the diodes ZnO film. Furthermore, in a recent study by Labram *et al* ZnO was utilised in conjunction with $Ga_2O_3$ to prepare resonant tunnelling diodes (RTD) [64]. Similar to the previously explained ZnO layer, which was spin coated from a ZnO hydrate precursor solution, the $Ga_2O_3$ layers were spin coated from a gallium nitrate hydrate solution. The $Ga(NO_3)_3 x H_2O$ was dissolved in water (12 mg ml$^{-1}$), spin coated in air, and annealed at 200 °C for 30 min. For a solution processable ZnO layer that is compatible with low-Tg plastic substrates the high temperature annealing step should be circumvented. To accomplish this for future device fabrication, a metal oxide nanoparticle dispersion could be utilised. Like zinc oxide, solution deposition has been used for other metal oxide films for various electronic applications. This includes, but is not limited to, molybdenum trioxide [72] and tungsten trioxide [73] solutions, which were both used with low temperature annealing in organic photovoltaics.

Other components of the diode architecture have been printed, in addition to the semiconducting diode layers, including the top electrode. A summary of printed conductive inks used as the top electrode of diodes is found in table 2.

## 4. Circuits and switching

Circuits based on diodes leverage the rectifying properties of diodes. Most literature on printed/organic diode

**Table 2.** Printed electrodes used in diode fabrication.

| Material | Function | Printing method | Device structure |
| --- | --- | --- | --- |
| Silver flake ink [56, 58] | Top electrode (bottom electrode: Cu on PET) | Gravure printed | PET/Cu/PTAA/Ag |
| Carbon and Ag paste [65] | Top electrode | Screen printed | PET/Al/SU8:Sb-Si/SU8:NbSi$_2$/carbon paste/Ag |
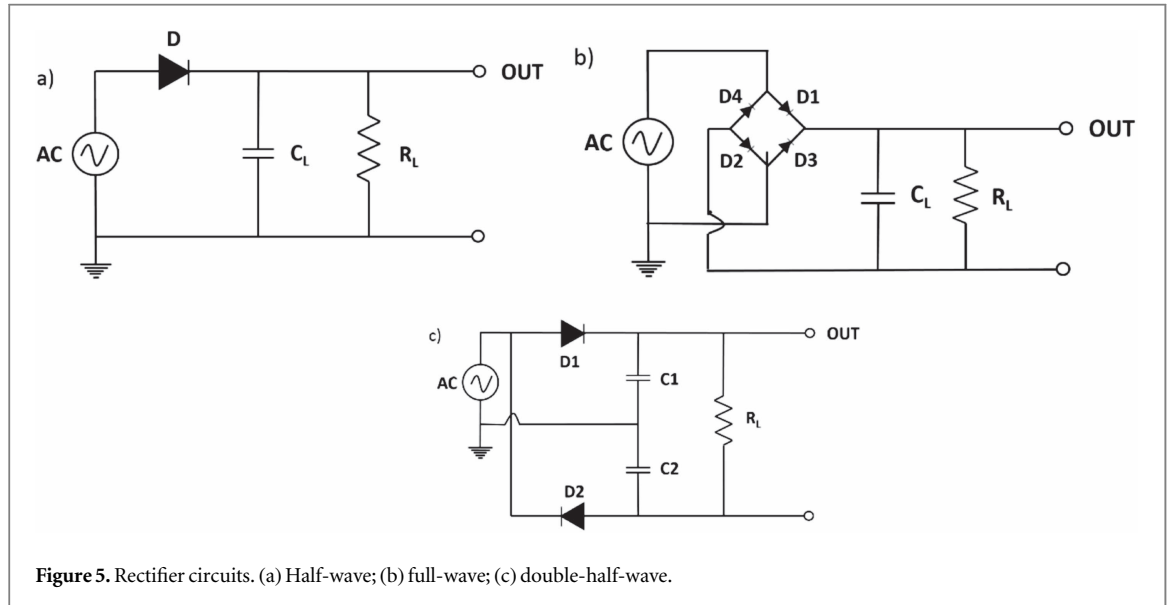


**Figure 5.** Rectifier circuits. (a) Half-wave; (b) full-wave; (c) double-half-wave.

based circuits focuses on conversion of an AC to a DC voltage for the purpose of generating a DC signal or for harvesting of AC energy, though at the end we will briefly look at a potential application in display backplanes.

Much of the initial work on rectifier circuits was performed when interest in fully printed radio frequency identification (RFID) tags was very high. As a result, the key task was to convert the oscillating electromagnetic field into a dc voltage for the purpose of driving on-board circuitry. For this purpose, the rectification ratio should be good but it is not as critical a parameter as the switching speed, i.e. the speed with which the diodes in the circuit can react to a change in incoming signal. Far beyond the maximum switching speed, the diode operates only as a geometric capacitor and cannot rectify a signal.

Various rectifier circuits have been reported. The simplest consists only of a diode in series with a smoothing capacitor in parallel with a load resistance and is called a half-wave rectifier figure 5(a), since only one half of the incoming signal is passed through. Many of the reported results on rectifiers have been obtained with this simple circuit. A full-wave rectifier is shown in figure 5(b), which is significantly more complex, and in figure 5(c) a double half-wave rectifier is shown, which can extract energy from both the positive and negative branches of the input AC signal but is still relatively simple to fabricate. Rectifiers fabricated from transistors are also reported in the literature but are beyond the scope of this review.

A simple upper limit expression for the switching speed of a diode in a simple rectifier circuit relates the switching speed to the transit time for charge carriers to traverse the semiconductor layer, given by

$$f_{max} = \frac{1}{t_T} = \frac{\mu(V_{IN} - V_{DC})}{d^2},\qquad(5)$$

where $\mu$ is the charge carrier mobility and $d$ is the semiconductor layer thickness. However, Steudel *et al* [53] argued that this approach, based on a small signal analysis is too simplistic in the case of high input and output voltages, and proposed an alternative model. In their analysis, the maximum frequency is based on the relationship between the charges needed by the load in one cycle and the charges delivered by the diode in one charging cycle and given by

$$\frac{V_{DC}}{R_L}\frac{2\pi}{\omega}\int_{t_2}^{t_2} I_{diode\_forward}\, dt,\qquad(6)$$

where SCLC is assumed. While this approach appears to work well for the evaporated pentacene diodes reported in [53], it is less clear whether this works as well for printed (and thus thicker) diodes based on lower mobility materials. However, neither of these upper limit estimates consider the additional effect of the capacitance of the printed diode itself, which can be significant and, for large area, thin diodes at high frequencies, be comparable to the effect of transit time.

The performance of a rectifier circuit depends on a number of factors, such as the effectiveness of switching at the target frequency, the load into which the

**Table 3.** Output of some organic rectifier circuits at or close to 13.56 MHz. Some of the published results are left outside due to the inadequate provided information for the comparison.

| Frequency (MHz) | Input voltage (V) | Output load (Ω) | Output voltage (V) | Rectifier type | SC material | Fabrication method | Reference |
|---|---|---|---|---|---|---|---|
| 14 | 18 | 50 k | 11 | H-W, diode | Pentacene | Vacuum | [53] |
| 14 | 5 | 1 M | 2 | H-W, diode | CuPc | Vacuum | [74] |
| 13.56 | 10 | 1 M | 4 | H-W, diode | PQT-12 | Spin-coating | [54] |
| 13.56 | 10 | 1 M | 3.5 | H-W, diode | PTAA | Printing | [59] |
| 13.56 | 11 | 1 M | 14.9 | Double H-W, diode | Pentacene | Vacuum | [75] |

signal is fed, and losses in the circuit e.g. from series resistance in the diode, which can be significant for low-mobility, undoped materials. A common figure is the 3 dB point, which is the frequency at which the dc output is reduced 3 dB from the maximum signal, but for a full performance assessment the maximum output is also needed. It is frequently challenging to compare different literature reports because the reporting of conditions is often incomplete. Table 3 below shows some results for rectifiers at or close to the HF RFID frequency of 13.56 MHz for which sufficient data was available for a comparison.

The choice of rectifier circuit for a given application needs to consider the specific non-ideal properties of printed and organic diodes. Heljo *et al* [59] investigated both half-wave and full-wave printed rectifiers based on PTAA. Although the full-wave configuration could in principle harvest more energy from the incoming AC signal than the half-wave, the voltage drop over the diodes led to a reduced overall output from the full-wave circuit. However, the output signal was smoother with a full-wave rectifier so that for applications requiring low ripple the full-wave might still be a good option.

While much earlier work on RF rectifiers was aimed at fully printed HF RFID tags, optimism for fully printed RFID tags has faded significantly, though there is still strong interest in printed NFC tags [76]. On the other hand, RF is a potential source of energy for powering distributed energy autonomous sensors. Lehtimäki *et al* [77] demonstrated an energy harvesting system consisting of a printed rectifier and aqueous supercapacitors: the system was charged by a commercial 13.56 MHz RFID reader, and was able to run a low power ASIC for close to 11 h on the energy harvested by the rectifier and stored in the supercapacitors.
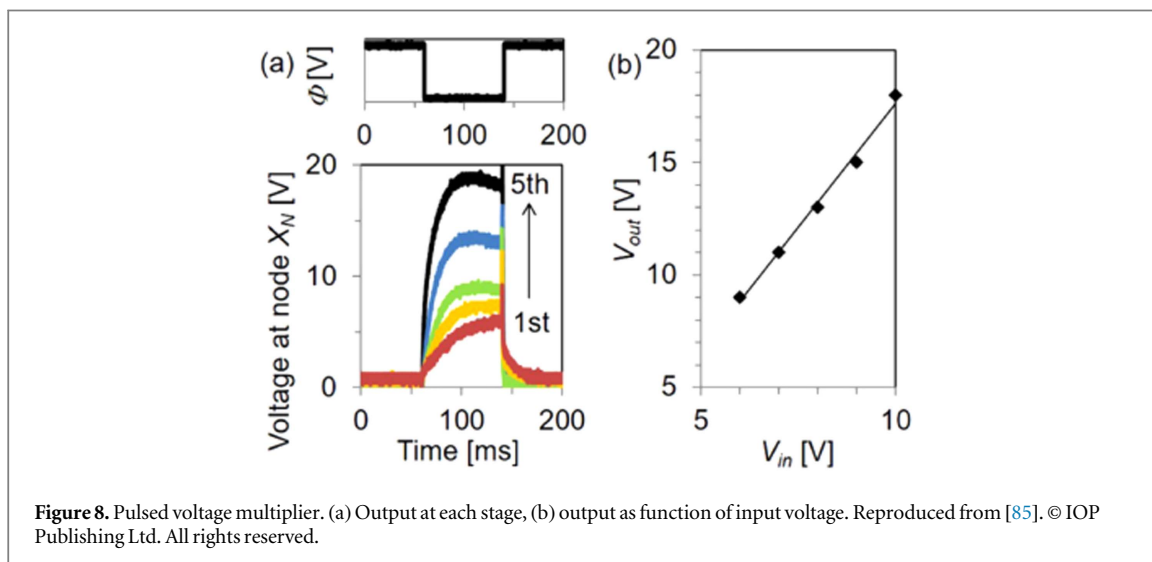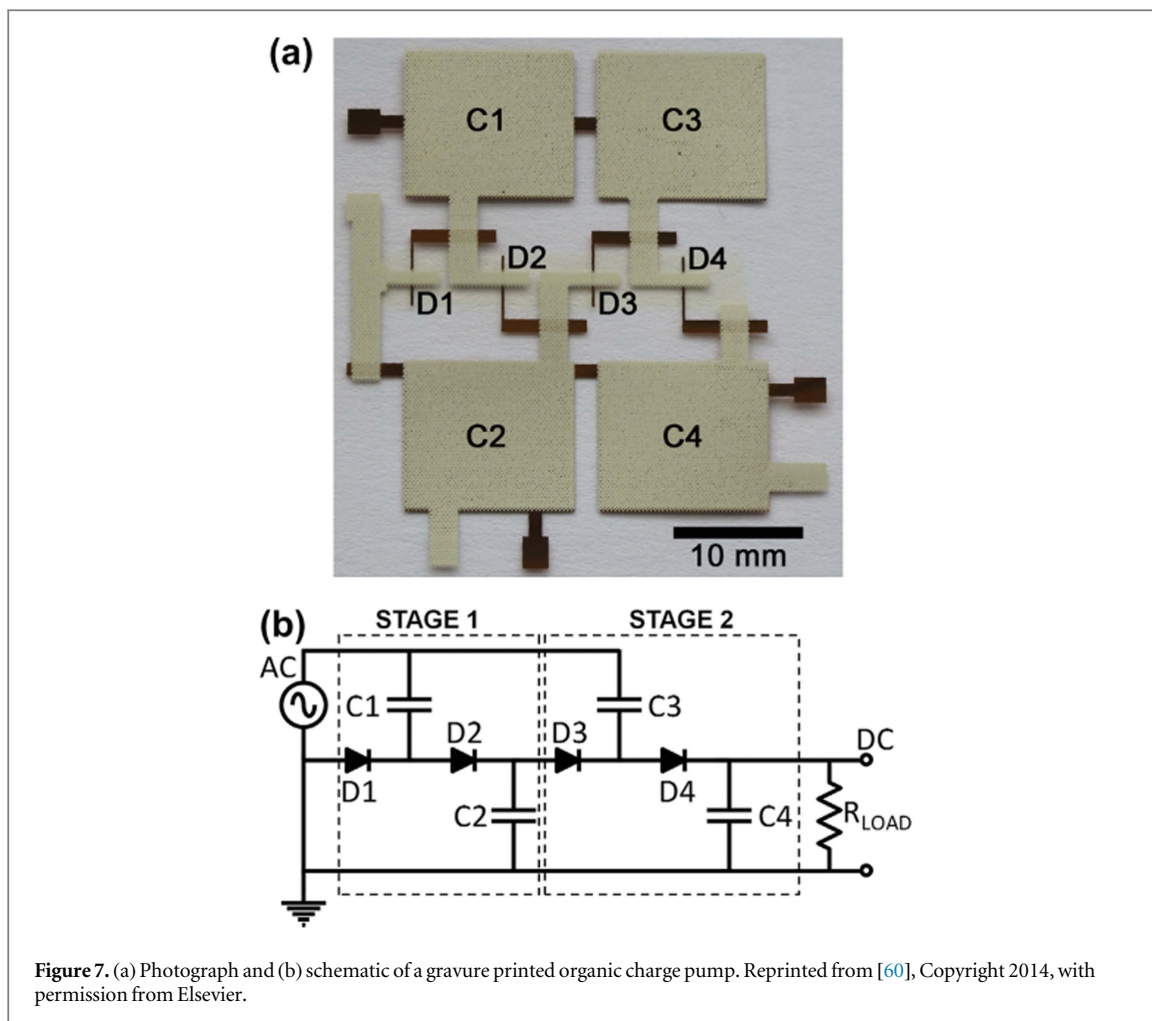
An issue with RF harvesting is that much of the RF energy available is at relatively high frequencies, in the GHz or slightly below range, e.g. cell phone systems, UHF RFID and Wifi. This has traditionally presented a severe challenge for printed diodes, but there has been significant progress recently. The first report of an organic diode rectifying at close to 1 GHz was from Steudel *et al* [78]. They reported rectification up to 869 MHz (approximately the 3 dB point) in a half-wave rectifier made of evaporated pentacene on a
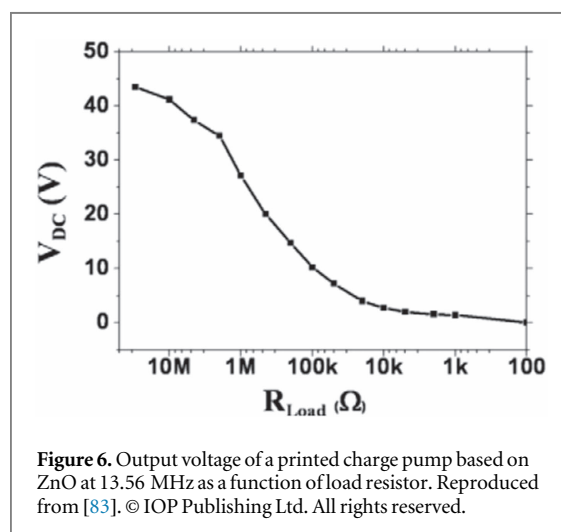


**Figure 6.** Output voltage of a printed charge pump based on ZnO at 13.56 MHz as a function of load resistor. Reproduced from [83]. © IOP Publishing Ltd. All rights reserved.

flexible substrate. However, there were no printing or solution processing steps in this circuit. Kleeman *et al* [48] reported a half-wave rectifier from the pentacene/C60 p–i–n diode discussed in section 2. Based on the published figures the 3 dB point was around 100 MHz but significant rectification was observed up to the measurement limit of 300 MHz, with the authors extrapolating to expectations of ability to rectify up to 1 GHz.

The first report of a printed rectifier operation above 1 GHz, to our knowledge, was by Sani *et al* in 2014 [65]. The diodes consisted of layers of ground up Si wafers dispersed in SU8 photopolymer followed by ground up conductive NbSi$_2$, also dispersed in SU8, situated between Al/Al$_2$O$_3$ and carbon/Ag electrodes. It is not possible from the paper to determine the power harvesting efficiency or what kind of rectifier circuit or load resistor was used, the 3 dB point appeared to be close to 1.6 GHz. The authors were able to use the RF signal from a mobile phone during a call (carrier frequency 1.8 GHz) to switch a small electrochromic display element, but quantitative information is difficult to extract from the report. Still, this is the first definitive demonstration of effective rectification above 1 GHz in a fully printed rectifier. More recently, the same group [79] reported a simpler manufacturing method based on the lamination of a freestanding composite film of Si microparticles, glycerine and nanofibrillated cellulose between an Al Schottky

**Figure 7.** (a) Photograph and (b) schematic of a gravure printed organic charge pump. Reprinted from [60], Copyright 2014, with permission from Elsevier.



**Figure 8.** Pulsed voltage multiplier. (a) Output at each stage, (b) output as function of input voltage. Reproduced from [85]. © IOP Publishing Ltd. All rights reserved.

contact and a Ni coated carbon Ohmic contact. They were able to demonstrate a cut-off frequency of 1.8 GHz and studied the maximum power point for energy harvesting using a variable load resistance.

Solution processed metal oxides are also promising materials for high-speed diodes, as they exhibit high charge carrier mobility, and processing temperatures, while not ready for sensitive polymers such as PET, have reached levels compatible with polyimide. Georgiadou *et al* [46, 80] measured the frequency response of the nanogap ZnO diodes discussed in section 2 and found no loss in dc output at all up to the measurement limit of 20 MHz. Based on the geometry of the devices and the mobility of the material, switching frequencies
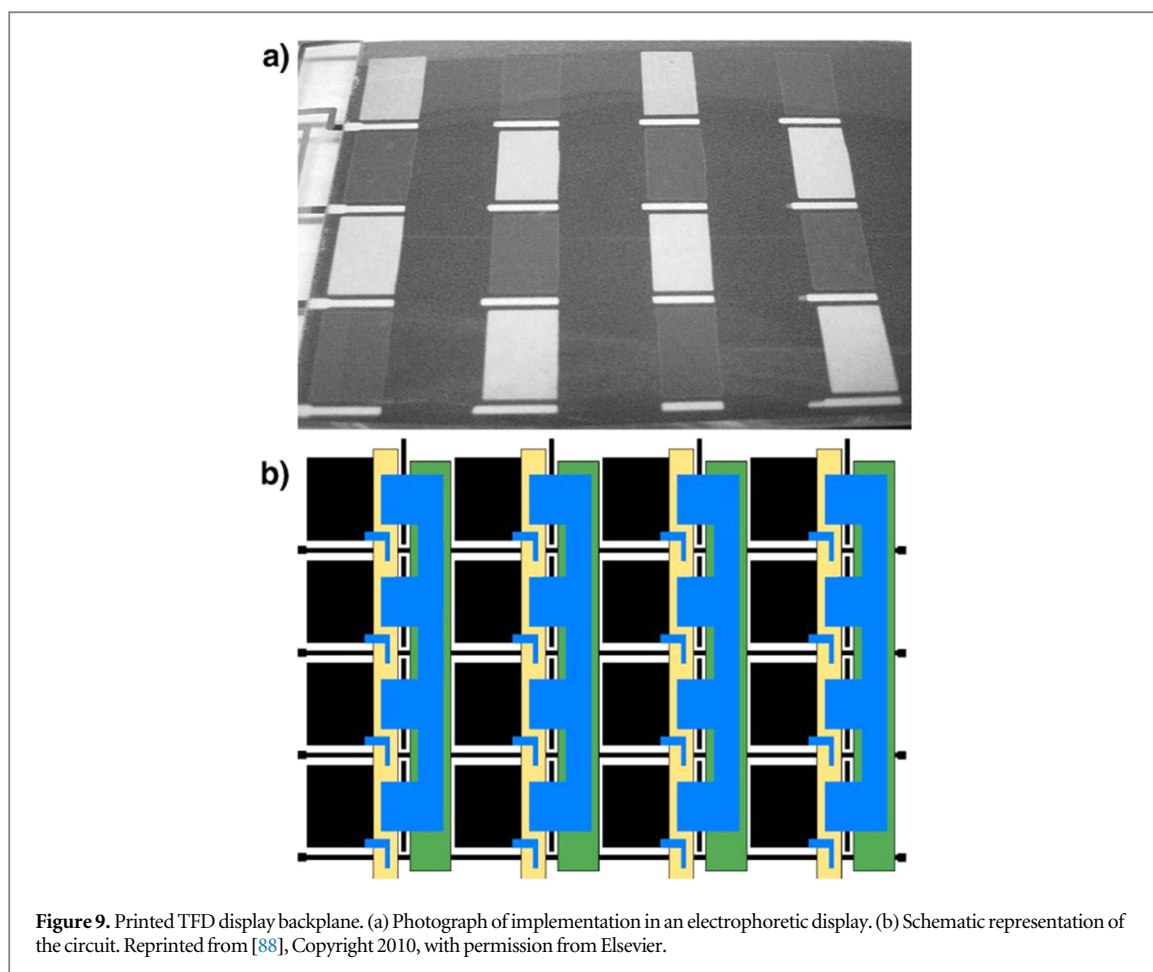
**Figure 9.** Printed TFD display backplane. (a) Photograph of implementation in an electrophoretic display. (b) Schematic representation of the circuit. Reprinted from [88], Copyright 2010, with permission from Elsevier.

well into the GHz range are expected. However, detailed descriptions of rectifier circuit and performance or of energy harvesting have not been published.

While standard rectifiers are useful circuits for creating a relatively low DC voltage or for harvesting energy from an RF field, the situation also arises in which very little current is needed to drive a high input impedance device, but a voltage higher than the input AC voltage is needed. In this case a charge pump circuit can be implemented as a voltage multiplier. The first organic diode based charge pump was reported by Mutlu *et al* [81], who fabricated a single stage charge pump based on drop cast P3HT with electrodes patterned by photolithography and shadow mask. The DC output was not larger than the AC input, but an improvement over the expectation of a simple rectifier circuit was achieved. However the DC output began to decrease already after ca 1 kHz. The following year, Heljo *et al* [82] reported a two stage charge pump based on gravure printed PTAA diodes and inkjet printed capacitors, which yielded 18 V DC from a 10 V AC input up to ca 1 MHz and just over 10 V DC at 13.56 MHz. Park *et al* [83] reported a fully printed rectenna including charge pump circuit operating at 13.56 MHz in 2012, using ZnO as semiconductor. They integrated this into a 1 bit RFID transponder as well [84] At very high load resistance they were able to obtain over 40 V DC from a 20 V AC input, but the

output voltage dropped rapidly with load resistance figure 6. This is a general issue with printed charge pumps, which are designed to deliver voltage rather than current.

Heljo *et al* [60] reported a fully gravure printed two stage charge pump in 2013. A pre-patterned backplane of Cu on PET formed the diode cathode, capacitor bottom electrode, and interconnects. PTAA and PMMA were gravure printed as diode semiconductor and capacitor dielectric, respectively, and a silver-flake ink was printed as diode anode and capacitor top electrode. The circuit and a photo of the charge pump are shown in figure 7. While the performance was not quite as good at 13.56 MHz and 1 MΩ load as the circuit prepared by heterogenous integration of gravure printed diodes and inkjet printed capacitors, the fabrication process for this monolithically integrated circuit was much simpler. Nonetheless, the input voltage was almost doubled at low frequency, and the output of 8.4 V DC for a 10 V AC input at 13.56 was significantly better than could be achieved with a simple rectifier circuit. For a 10 MΩ load ca 12 V DC could be extracted from a 10 V AC input at 13.56 MHz.

The charge pump circuits described above are useful for converting an AC voltage to a higher DC voltage. However, for circuits operating from a DC power which need only a short pulse at higher voltage, another approach is needed. Recently, Ng *et al* [85]

reported a fully inkjet printed pulsed voltage multiplier comprising a transistor based pulse generator and a PTAA diode based voltage multiplier. With this configuration they were able to demonstrate multiplication of the generated pulse (see figure 8).

A very different application from AC/DC converters and voltage pumps is the area of display backplanes. While the standard approach for high resolution active matrix displays is the use of thin-film transistors (TFTs), TFTs offer the potential for lower cost manufacturing due to the simpler architecture. This was a significant field of activity in the 1990s [86] and MIMS were used for some time in mobile phone displays. The subject arose more recently again as Amorphyx announced TFT backplane technology based on amorphous metal films [87]. The simplicity of printed organic MIM diodes makes the TFT approach attractive for cost-sensitive applications, e.g. in signage, where extremely high resolution is not needed. In the case of a TFT backplane, especially for e-paper type displays in signage, fast switching is not needed, in contrast to RF rectification. On the other hand, the rectification ratio, which must be relatively modest for RF rectification, is critical to avoid crosstalk in the display. There have not been many reports of printed TFTs for display backplanes, but Lilja *et al* [88] and Virtanen *et al* [89] reported a circuit, driving scheme and simple implementation of a backplane for an electrophoretic display (figure 9).
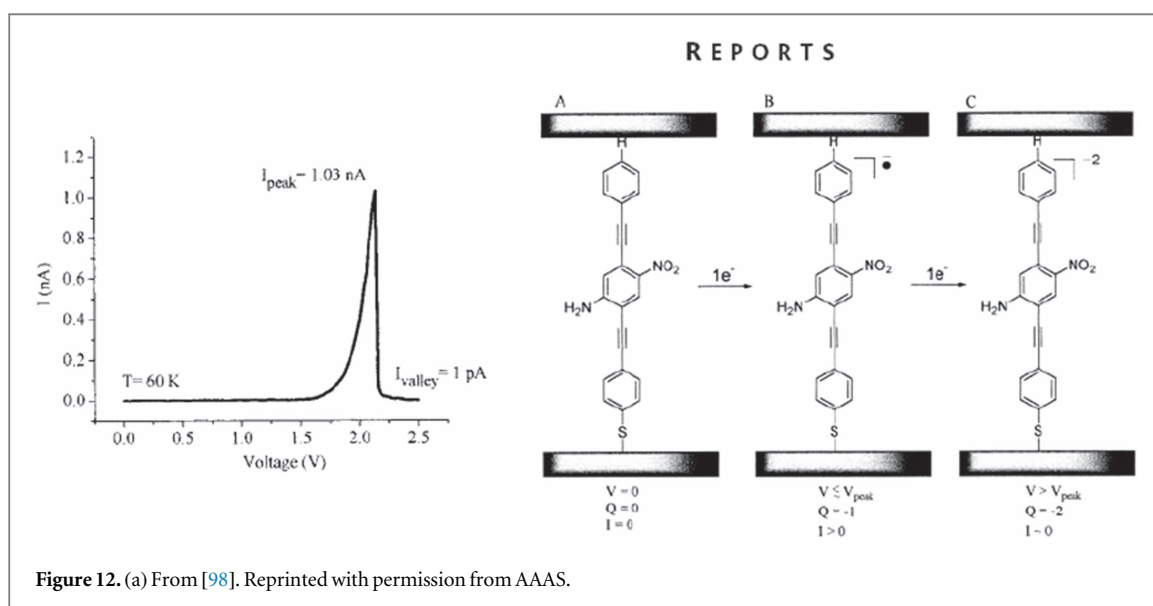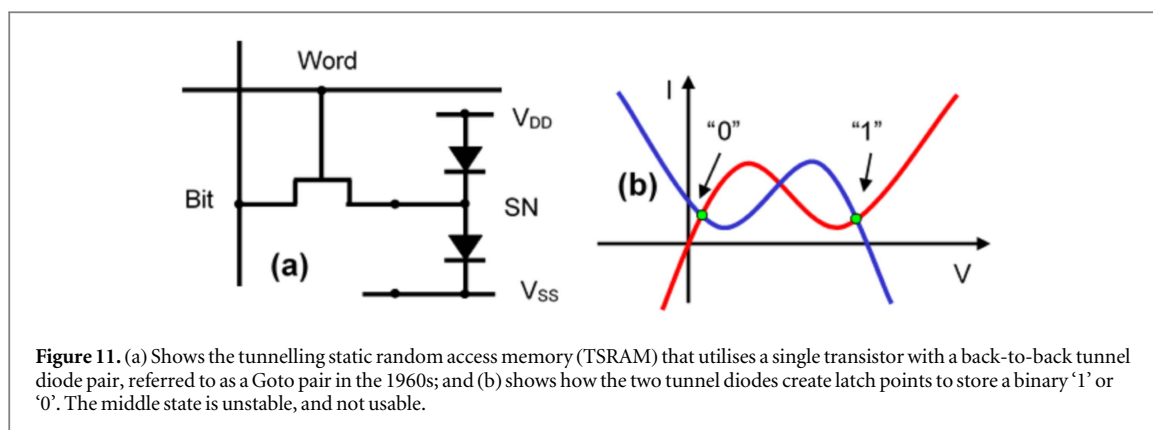
## 5. Tunnel diodes

A particular subset of diodes with unique properties that can translate to potentially impactful low-energy hybrid transistor/diode circuits are called tunnel diodes. As revealed in Leo Esaki's Nobel prize winning work [90], quantum mechanical tunnelling through a thin barrier with quantum selection rules imposed by the allowed density-of-states (DOS) and carrier populations of the multilayer system, leads to negative differential resistance (NDR). The manifestation of NDR in a diode is when the *I–V* characteristics resembles a capital letter 'N', whereby it first rises in current with increasing voltage bias, figure 10(a), but then falls in current with additional voltage bias, shown between figures 10(b) and (c), called the 'NDR region', before finally rising again as conventional diffusion current becomes exponentially significant (see figure 10(d)). There are many circuit topologies that span memory [91–93], logic [94], and mixed-signal [95] that can be enhanced by these hybrid tunnel diode/transistor circuits, reducing device count, lowering parasitic delays and dropping power consumption (see figure 11 as TSRAM example). Indeed, since quantum tunnelling is significantly faster than conventional drift or diffusion currents, inorganic tunnel diodes have reached oscillation frequencies in excess of 2 THz [96]. For a more comprehensive discussion
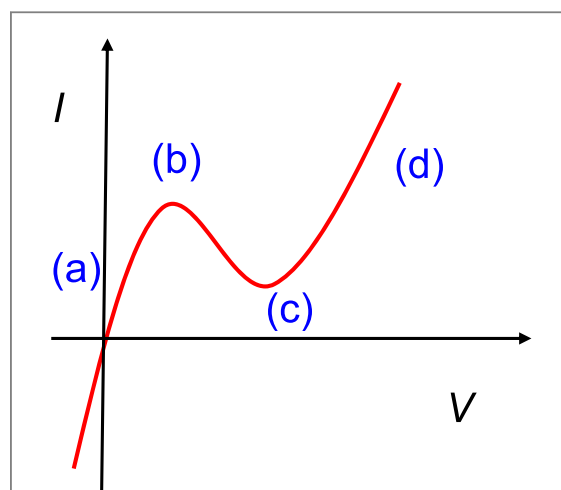


**Figure 10.** As shown, a quantum tunnelling current superimposed upon the normal diode diffusion current creates a rise in current at low voltages (a), followed by a peak at (b) where the tunnelling probability peaks due to energy level overlaps, and then followed by the NDR between (b) and (c). The normal diffusion current raises the current again at (d). The PVCR is a unitless metric derived by dividing the current at (b) by the current at (c).

of NDR devices and circuits, please see Berger and Ramesh [97]. But, most reports of diodes with NDR properties are relegated to the inorganic semiconductor community. Treated here is a brief review of some diodes that manifest NDR and fall within the category of having been printed, or could easily be seen as print compatible in the near future.

One of the first reports of NDR behaviour with organic molecules was reported by Reed and Tour [98], where a thin gold wire was stretched until it finally broke, leaving a nanometre sized gap in between. Then the 'break wire' was immersed in a solution with conducting molecules whose terminations were thiol units, which have a significant chemical affinity for gold bonding. Thus, if all went well, a single molecule would bridge the break wire gap, but sometimes two or three molecules. When the voltage bias was swept upwards, the measured current exhibited NDR. And the measured NDR had a peak-to-valley current ratio (PVCR) that exceeded 1000, when many NDR hybrid circuits can operate well with a PVCR exceeding 2, although higher PVCR is perceived as optimal (see figure 12). With a larger PVCR, it is implied that the valley current becomes low, thus reducing the static power consumption. However, if the PVCR is high, leading to a high peak current density, then the dynamic power consumption to switch a digital latch from one state to another, over the NDR hump, will also become momentarily larger in order to overcome this large peak current. One criteria often overlooked with NDR devices is that in order to form latches from pairs of back-to-back tunnel diodes, as noted in tunnelling static random access memory (TSRAM) [92], after the NDR region, the current must increase again, to complete the capital letter 'N' shape,

**Figure 11.** (a) Shows the tunnelling static random access memory (TSRAM) that utilises a single transistor with a back-to-back tunnel diode pair, referred to as a Goto pair in the 1960s; and (b) shows how the two tunnel diodes create latch points to store a binary '1' or '0'. The middle state is unstable, and not usable.



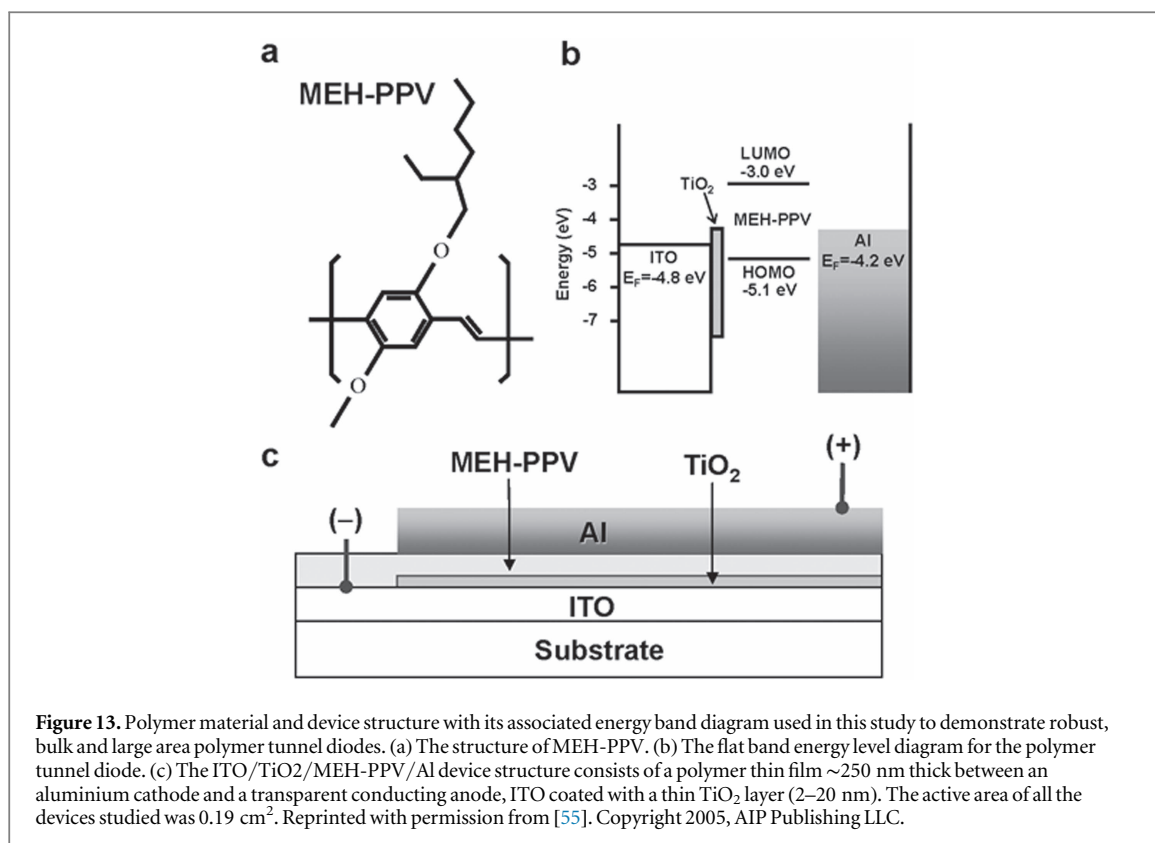**Figure 12.** (a) From [98]. Reprinted with permission from AAAS.

in order to form the second critical latch state. These early 'break wire' molecular diodes only spiked up and then back down, therefore they were unsuitable for hybrid transistor/tunnel diode circuits.

But in 2005, the first report of a potentially printable organic tunnel diode was made using a single thin metal-oxide tunnelling barrier between the anode and a relatively thick organic semiconductor [55], shown in figure 13. Since the metal-oxide tunnelling barrier defines the majority of the NDR, the thickness of the organic semiconductor becomes less relevant, and thus relaxes the constraint on thickness, rendering it printable in the future. In this early report, the shape of the I–V characteristic was indeed a capital letter 'N', and it even showed latching and storage of a single bit through a breadboarded circuit with an NMOS transistor. The metal oxide tunnelling barrier was comprised of $TiO_2$ metal oxide, synthesised by evaporation of pure Ti metal, followed by oxygen plasma oxidation, as shown in figure 13(b). In order for NDR to manifest itself, it is not only quantum mechanical tunnelling, but the boundary constraints imposed on the tunnelling selection rules through the allowed and disallowed energy states. A well defined quantised energy

state(s) allows better NDR performance. It was speculated that a reported oxygen vacancy defect level created an energy level in the $TiO_2$ forbidden energy gap, below its conduction band, acted as a 'keyhole' through which carriers tunnelled into the DOS in the organic semiconductor's LUMO [99]. In this report, room temperature NDR was measured up to 53, was repeatable over many devices, and there was not any significant hysteresis with forward and backward sweeps, as shown in figure 14. However, one deviation from a traditional Esaki tunnel diode was that the peak tunnelling current density did not increase exponentially as the metal-oxide tunnelling barrier was thinned linearly from 2 to 10 nm. So, it was postulated that the tunnelling occurred through this extended oxygen vacancy defect through a successive capture and reemission.

It should be noted that reports of memristors using $TiO_2$ with oxygen vacancies might bare some resemblance [100, 101] to Yoon *et al* [55]. In a memristor, oxygen vacancies are embedded in half the $TiO_2$ active region cube. By the application of an external bias, the charged oxygen vacancies diffuse across the $TiO_2$, which is sometimes 40 nm thick. Essentially the

**Figure 13.** Polymer material and device structure with its associated energy band diagram used in this study to demonstrate robust, bulk and large area polymer tunnel diodes. (a) The structure of MEH-PPV. (b) The flat band energy level diagram for the polymer tunnel diode. (c) The ITO/TiO2/MEH-PPV/Al device structure consists of a polymer thin film ~250 nm thick between an aluminium cathode and a transparent conducting anode, ITO coated with a thin $TiO_2$ layer (2–20 nm). The active area of all the devices studied was 0.19 cm$^2$. Reprinted with permission from [55]. Copyright 2005, AIP Publishing LLC.
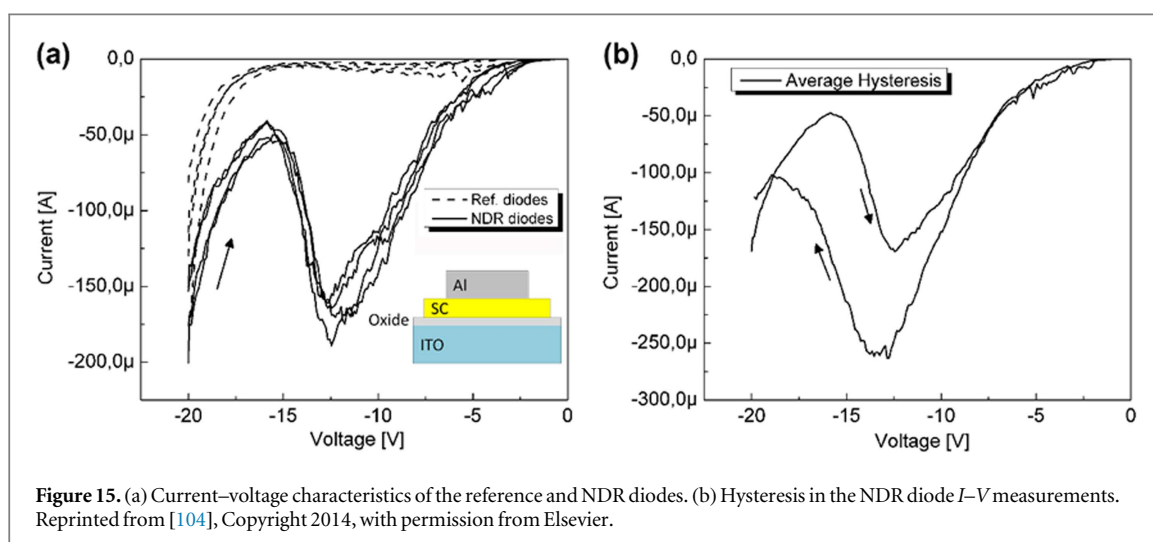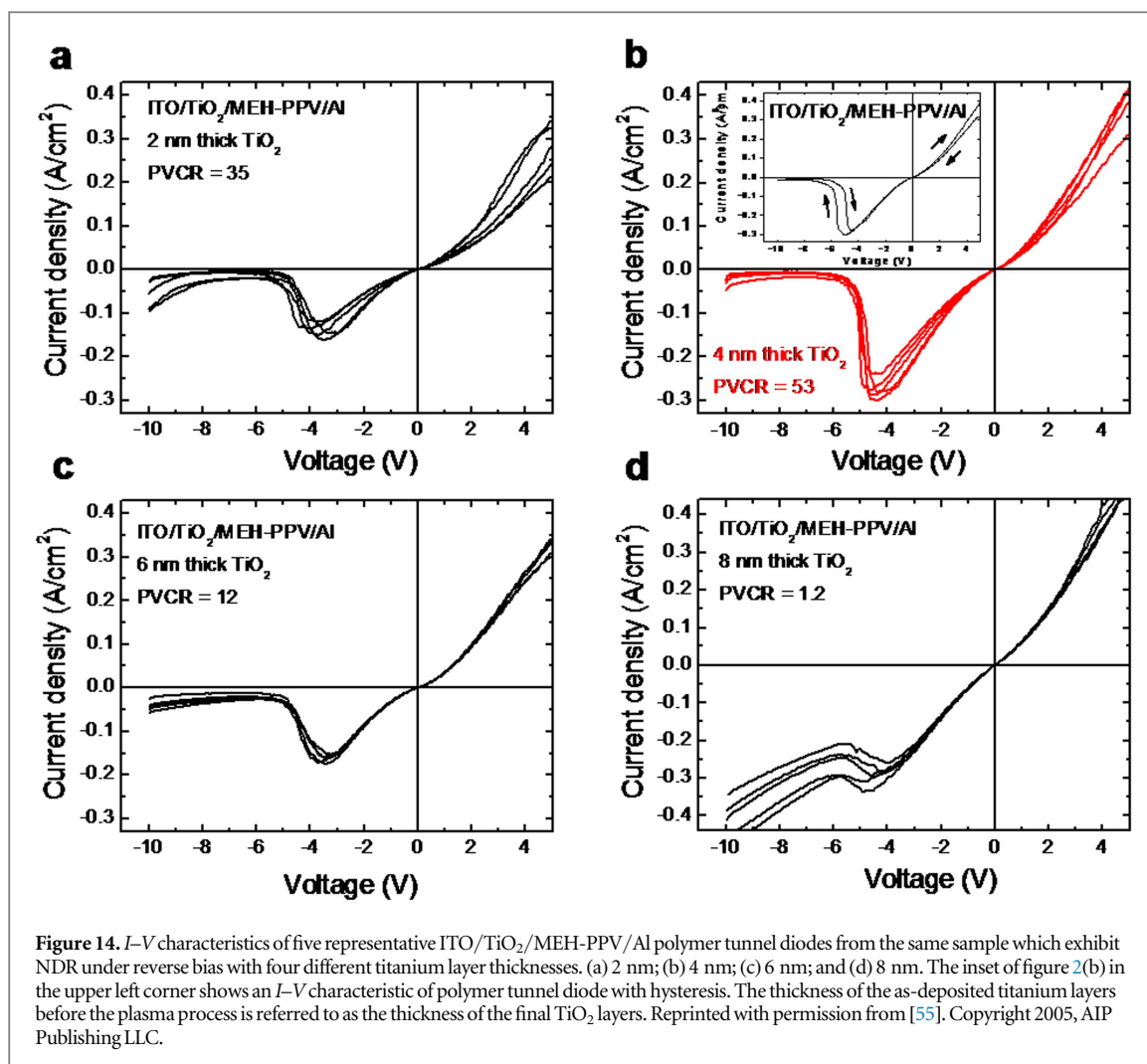
oxygen vacancies act as dopants, altering the $TiO_2$ cube's resistivity from a low conducting state, to a high conducting state. And when the bias is reversed, the charged oxygen vacancies are repelled, rendering the $TiO_2$ cube more resistive. Thus, a memristor lacks a true NDR region, but simply switches between two resistive states spanning the *I–V* origin, cycling between a steep slope for low resistance, and a shallow slope for high resistance. Most recent memristor reports eliminated the Langmuir–Blodgett films and now are synthesised entirely from metal-oxides, like $TiO_2$, sandwiched between electrodes, such as platinum. Thus, there are also no DOS selection rules imposed by a semiconductor with a forbidden energy gap. Therefore, this class of devices is wholly distinct from the organic/inorganic tunnelling diodes. But, it could be possible that some memristor-like behaviour could be superimposed onto the NDR [55] if the $TiO_2$ used in Yoon's work [55] was not saturated with oxygen vacancies.

An alternate approach to achieving NDR with printable diodes was presented by Labram *et al* [64]. This particular example emulated a RTD, which is another NDR generating diode put forth by Tsu and Esaki [102, 103] that creates its NDR by the alignment of bulk carriers with a quantum confined energy state in a thin crystalline semiconductor, sandwiched between two quantum mechanically thin energy barriers. The barriers must be thick enough to confine the electron wave function within the central semiconductor, but thin enough to allow a high probability for electron tunnelling through the barriers. Labram *et al*'s approach was

to use spin-cast layers of ZnO from precursor form for the semiconductor elements. These were subsequently sintered at temperatures $\leqslant 200\ ^\circ C$ to promote crystallinity. One type of NDR diode reported here used 2 nm thick spin-cast ZnO with 2 nm thick $Ga_2O_3$ barriers. For the $Ga_2O_3$ barriers, they were also added from spin-cast materials applied in precursor form and annealed for conversion to a crystalline, or semi-crystalline, form. These diodes did display some NDR behaviour, albeit quite noisy and somewhat irregular. Having both the quantum well and quantum barriers synthesised by spin casting, which leads to non-uniform thicknesses, as evidenced by their high resolution transmission electron microscope image, leads to a smearing of the energy levels that will shift the NDR peak voltage and its PVCR performance both within a diode and between adjacent diodes.
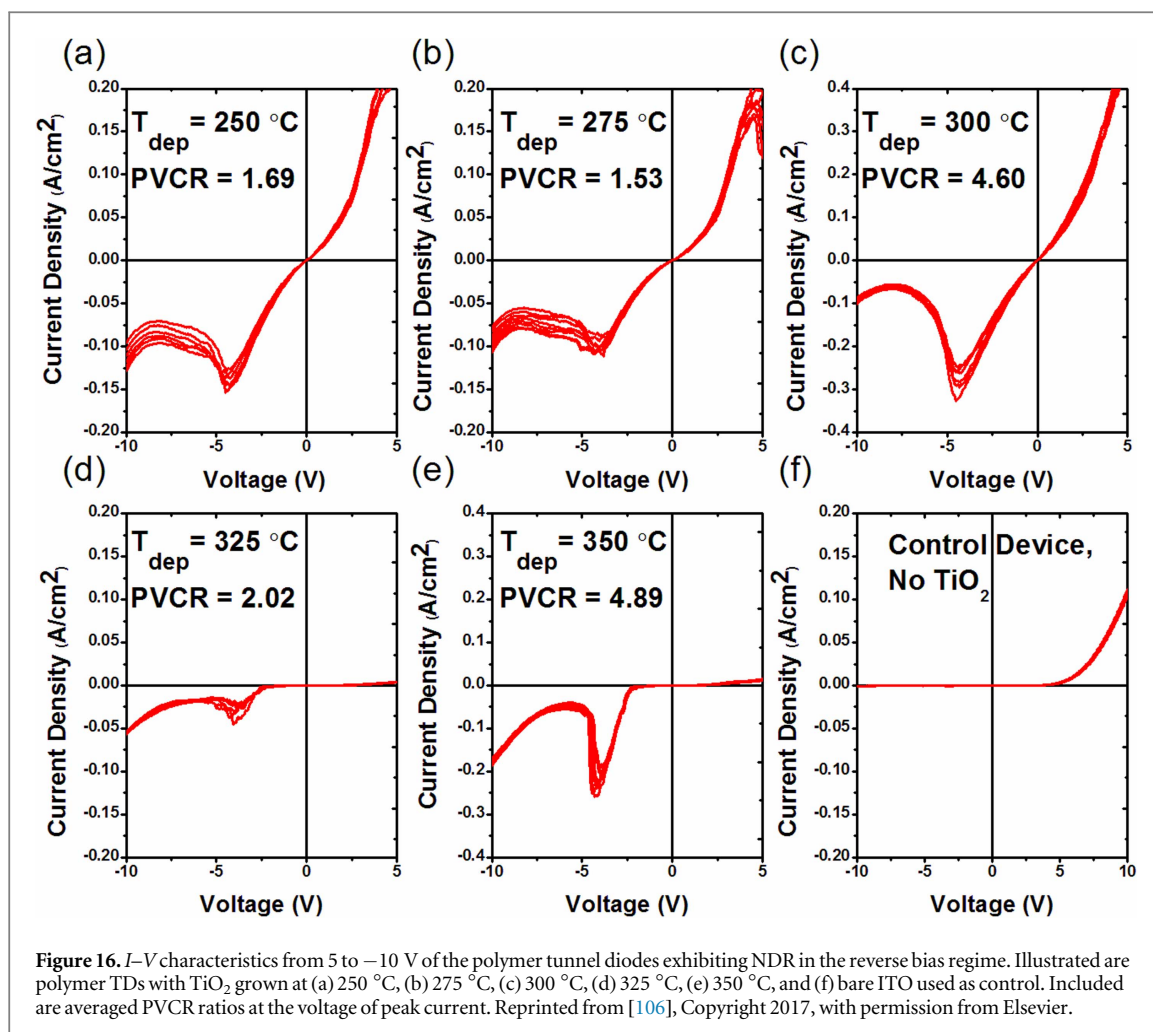
A more promising printable NDR diode was also presented by Labram *et al* [64] that replaced the $Ga_2O_3$ barriers with self-assembled monolayers (SAM). The SAM layers should be more consistent in morphology and thickness, thus leading to enhanced NDR behaviour over the $Ga_2O_3$ barriers. Here the modified *I–V* characteristics presented lacked appreciable noise and illustrated repeatable NDR across multiple sweeps of a single diode. This could be a promising approach to realise printable NDR devices, but the crystallinity of the spin-cast ZnO quantum well will still present some challenges by smearing the confined energy state from the thickness uniformity and the variable crystallinity of the quantum well of spin-cast and sintered films.

**Figure 14.** *I–V* characteristics of five representative ITO/TiO₂/MEH-PPV/Al polymer tunnel diodes from the same sample which exhibit NDR under reverse bias with four different titanium layer thicknesses. (a) 2 nm; (b) 4 nm; (c) 6 nm; and (d) 8 nm. The inset of figure 2(b) in the upper left corner shows an *I–V* characteristic of polymer tunnel diode with hysteresis. The thickness of the as-deposited titanium layers before the plasma process is referred to as the thickness of the final TiO₂ layers. Reprinted with permission from [55]. Copyright 2005, AIP Publishing LLC.



**Figure 15.** (a) Current–voltage characteristics of the reference and NDR diodes. (b) Hysteresis in the NDR diode *I–V* measurements. Reprinted from [104], Copyright 2014, with permission from Elsevier.

Returning to the earlier report of an organic diode with a single thin TiO₂ tunnelling barrier, Heljo *et al* [104] modified the earlier fabrication process flow, keeping the intrinsic tunnel diode topology, but extending the synthesis of the thin metal oxide tunnel barriers through anodic oxidation. In this work, the organic semiconductor MEH-PPV was

replaced with PDY-232, which was simply easier to process, but has commensurate electronic properties. Shown in figure 15, is the NDR characteristics of this diode with strong NDR, albeit with some noise. A PVCR up to 3.6 was recorded at room temperature, but the peak voltage increased to about −12 volts. Some hysteresis was measured, perhaps emblematic

**Figure 16.** *I–V* characteristics from 5 to −10 V of the polymer tunnel diodes exhibiting NDR in the reverse bias regime. Illustrated are polymer TDs with $TiO_2$ grown at (a) 250 °C, (b) 275 °C, (c) 300 °C, (d) 325 °C, (e) 350 °C, and (f) bare ITO used as control. Included are averaged PVCR ratios at the voltage of peak current. Reprinted from [106], Copyright 2017, with permission from Elsevier.

of partial memristor-like behaviour, as the $TiO_2$ may not be saturated with oxygen vacancies via anodic oxidation.

A preliminary report by Guttman *et al* at the 2015 Fall MRS Meeting [105] and recently greatly expanding upon [106], has shown great efficacy for these tunnel diodes to technology transfer to atomic layer deposition (ALD) for the synthesis of the $TiO_2$ tunnelling barriers [105, 107]. Here oxygen vacancies were created by ALD deposition conditions by not using conventional deposition recipes, leading to slightly non-stoichiometric $TiO_2$ with some oxygen vacancies. As can be seen in figure 16, Guttman *et al* demonstrated polymer tunnel diodes with high room temperature NDR using an ALD deposited tunnelling layer deposited between 250 °C and 350 °C. A Picosun SUNALE R-150B ALD reactor fitted with a titanium tetrachloride (TiCl$_4$) precursor and $H_2O$ oxidiser was used for the $TiO_2$ deposition. A critical relationship between deposition temperature, oxygen vacancy concentration and room temperature NDR was presented. This report also shows how the diode's multilayer bands, especially the $TiO_2$ tunnelling barrier, align with the DOS of the LUMO of the PDY-132 organic semiconductor, as calculated by density functional theory. Interestingly, $TiO_2$ undergoes a phase change between 200 °C and 300 °C,

resulting in an obvious change in the microstructure of the crystals. According to literature, the films deposited near 300 °C are more than likely mixed phase between anatase and rutile while the rutile phase exists in $TiO_2$ films for ALD temperatures above 350 °C. For a $TiO_2$ deposition temperature of 350 °C, the peak NDR voltage position ($V_{peak}$) and associated peak current density ($J_{peak}$) were ∼4.13 V and −0.23 A cm$^{-2}$, respectively, with a PVCR as high as 4.89 while operating at room temperature. And for a $TiO_2$ deposition temperature of 250 °C, the minimum cracking temperatures of the TiCl$_4$ precursor to release the Ti atom, $V_{peak}$ and associated $J_{peak}$ were ∼4.3 V and −0.14 A cm$^{-2}$, respectively, with a PVCR of 1.69 at room temperature. The key advantages of the ALD process used in fabrication of PTDs are increased repeatability and manufacturability, and now with reduced temperature depositions possible, their compatibility with flexible substrates is greatly enhanced. This shows great promise for further scale up to printable hybrid circuits.

# 6. Conclusion

Although transistors have received more attention in the literature, diodes are extremely important active

devices with a wide range of applications. Solution processed and organic diodes can be fabricated from a wide range of organic and inorganic materials, as reviewed in this article. The physics of operation has been significantly better understood over the last 20 years or so, with the majority of devices well described by a MIM model but some devices also operating as p–i–n junction diodes. Progress in switching speeds has been significant, with even low-mobility materials operating well into radio frequencies and recent promising results in the GHz range. Progress has also been made in fabrication of reliable solution processed tunnel diodes for novel circuits. Applications for solution processed and organic diodes have included RFID, energy harvesting, voltage multiplication and display backplanes. Future progress will result from an integration of new materials combined with new fabrication processes and architectures. Diodes are far from dead!

## ORCID iDs

Thomas M Kraft ⓘ https://orcid.org/0000-0001-6017-0579
Paul R Berger ⓘ https://orcid.org/0000-0002-2656-2349
Donald Lupo ⓘ https://orcid.org/0000-0003-1686-5300

## References

[1] Basiricò L, Cosseddu P, Fraboni B and Bonfiglio A 2011 Inkjet printing of transparent, flexible, organic transistors *Thin Solid Films* **520** 1291–4
[2] Barret M, Sanaur S and Collot P 2008 Inkjet-printed polymer thin-film transistors: enhancing performances by contact resistances engineering *Org. Electron.* **9** 1093–100
[3] Chang J-F *et al* 2004 Enhanced mobility of poly(3-hexylthiophene) transistors by spin-coating from high-boiling-point solvents *Chem. Mater.* **16** 4772–6
[4] Baeg K-J *et al* 2011 Improved performance uniformity of inkjet printed n-channel organic field-effect transistors and complementary inverters *Org. Electron.* **12** 634–40
[5] Bao Z, Feng Y, Dodabalapur A, Raju V R and Lovinger A J 1997 High-performance plastic transistors fabricated by printing techniques *Chem. Mater.* **9** 1299–301
[6] Bao Z, Dodabalapur A and Lovinger A J 1996 Soluble and processable regioregular poly(3-hexylthiophene) for thin film field-effect transistor applications with high mobility *Appl. Phys. Lett.* **69** 4108
[7] Beecher P *et al* 2007 Ink-jet printing of carbon nanotube thin film transistors *J. Appl. Phys.* **102** 043710

[8] Kim D, Jeong S, Lee S H, Moon J and Song J K 2009 Ink-jet printing of organic semiconductor for fabricating organic thin-film transistors: film uniformity control by ink composition *Synth. Met.* **159** 1381–5
[9] Park K *et al* 2010 Stretchable, transparent zinc oxide thin film transistors *Adv. Funct. Mater.* **20** 3577–82
[10] Shao M, He Y, Hong K, Rouleau C M, Geohegan D B and Xiao K 2013 A water-soluble polythiophene for organic field-effect transistors *Polym. Chem.* **4** 5270
[11] Rogers J A, Bao Z and Raju V R 1998 Nonphotolithographic fabrication of organic transistors with micron feature sizes *Appl. Phys. Lett.* **72** 2716–8
[12] Wang C *et al* 2013 High performance thin film transistors based on regioregular poly(3-dodecylthiophene)-sorted large diameter semiconducting single-walled carbon nanotubes *Nanoscale* **5** 4156
[13] Zhao Y *et al* 2011 All-solution-processed, high-performance n-channel organic transistors and circuits: toward low-cost ambient electronics *Adv. Mater.* **23** 2448–53
[14] Yuan Y *et al* 2014 Ultra-high mobility transparent organic thin film transistors grown by an off-centre spin-coating method *Nat. Commun.* **5** 3005
[15] Haldar A, Liao K-S and Curran S A 2014 Fabrication of inkjet printed organic photovoltaics on flexible Ag electrode with additives *Sol. Energy Mater. Sol. Cells* **125** 283–90
[16] Yu G, Gao J, Hummelen J C, Wudl F and Heeger A J 1995 Polymer photovoltaic cells: enhanced efficiencies via a network of internal donor–acceptor heterojunctions *Science* **270** 1789–90
[17] Gan Q, Bartoli F J and Kafafi Z H 2013 Plasmonic-enhanced organic photovoltaics: breaking the 10% efficiency barrier *Adv. Mater.* **25** 2385–96
[18] Aernouts T, Aleksandrov T, Girotto C, Genoe J and Poortmans J 2008 Polymer based organic solar cells using ink-jet printed active layers *Appl. Phys. Lett.* **92** 033306
[19] Ratier B, Nunzi J-M, Aldissi M, Kraft T M and Buncel E 2012 Organic solar cell materials and active layer designs—improvements with carbon nanotubes: a review *Polym. Int.* **61** 342–54
[20] El Hajj A, Kraft T M, Lucas B, Schirr-Bonnans M, Ratier B and Torchio P 2014 Flexible inverted polymer solar cells with an indium-free tri-layer cathode *J. Appl. Phys.* **115** 033103
[21] Ahn S I *et al* 2012 OLED with a controlled molecular weight of the PVK (poly(9-vinylcarbazole)) formed by a reactive ink-jet process *Org. Electron.* **13** 980–4
[22] Blom P W M, Mihailetchi V D, Koster L J A and Markov D E 2007 Device physics of polymer:fullerene bulk heterojunction solar cells *Adv. Mater.* **19** 1551–66
[23] Lenes M, Morana M, Brabec C J and Blom P W M 2009 Recombination-limited photocurrents in low bandgap polymer/fullerene solar cells *Adv. Funct. Mater.* **19** 1106–11
[24] Dou L *et al* 2013 25th anniversary article: a decade of organic/polymeric photovoltaic research *Adv. Mater.* **25** 6642–71
[25] Pelzer K M and Darling S B 2016 Charge generation in organic photovoltaics: a review of theory and computation *Mol. Syst. Des. Eng.* **1** 10–24
[26] Chiechi R C, Havenith R W A, Hummelen J C, Koster L J A and Loi M A 2013 Modern plastic solar cells: materials, mechanisms and modeling *Mater Today* **16** 281–9
[27] Yan J and Saunders B R 2014 Third-generation solar cells: a review and comparison of polymer:fullerene, hybrid polymer and perovskite solar cells *RSC Adv.* **4** 43286–314
[28] Geffroy B, le Roy P and Prat C 2006 Organic light-emitting diode (OLED) technology: materials, devices and display technologies *Polym. Int.* **55** 572–82
[29] Thejo Kalyani N and Dhoble S J 2012 Organic light emitting diodes: energy saving lighting technology—a review *Renew. Sustain. Energy Rev.* **16** 2696–723
[30] Kataoka Y *et al* 2013 56.1: development of IGZO-TFT and creation of new devices using IGZO-TFT *SID Symp. Dig. Tech. Pap.* **44** 771–4

[31] Fortunato E, Barquinha P and Martins R 2012 Oxide semiconductor thin-film transistors: a review of recent advances *Adv. Mater.* **24** 2945–86

[32] Streetman B and Banerjee S 2015 *Solid State Electronic Devices* 7th edn. (Oxford: Pearson)

[33] Lilja K 2011 *Performance, Interfacial Properties and Applications of Printed Organic Diodes* (Tampere: Tampere University of Technology)

[34] Pan Stanford Publishing—Organic and Printed ElectronicsFundamentals and Applications, (Accessed 5 February 2017), http://panstanford.com/books/9789814669740.html

[35] de Bruyn P, van Rest A H P, Wetzelaer G A H, de Leeuw D M and Blom P W M 2013 Diffusion-limited current in organic metal–insulator–metal diodes *Phys. Rev. Lett.* **111** 186801

[36] Kuik M, Wetzelaer G-J A H, Nicolai H T, Craciun N I, De Leeuw D M and Blom P W M 2014 25th Anniversary article: charge transport and recombination in polymer light-emitting diodes *Adv. Mater.* **26** 512–31

[37] Wetzelaer G A H and Blom P W M 2014 Ohmic current in organic metal–insulator–metal diodes revisited *Phys. Rev. B* **89** 241201

[38] Leighton P A 1941 Electronic processes in ionic crystals (Mott, N F; Gurney, R W) *J. Chem. Educ.* **18** 249

[39] Schottky W 1938 Halbleitertheorie der Sperrschicht *Naturwissenschaften* **26** 843–843

[40] Nguyen P H, Scheinert S, Berleb S, Brütting W and Paasch G 2001 The influence of deep traps on transient current–voltage characteristics of organic light-emitting diodes *Org. Electron.* **2** 105–20

[41] Lilja K E, Majumdar H S, Pettersson F S, Österbacka R and Joutsenoja T 2011 Enhanced performance of printed organic diodes using a thin interfacial barrier layer *ACS Appl. Mater Interfaces* **3** 7–10

[42] Lilja K E *et al* 2011 Effect of dielectric barrier on rectification, injection and transport properties of printed organic diodes *J. Phys. Appl. Phys.* **44** 295301

[43] Cölle M, Büchel M and de Leeuw D M 2006 Switching and filamentary conduction in non-volatile organic memories *Org. Electron.* **7** 305–12

[44] Beesley D J *et al* Sub-15 nm patterning of asymmetric metal electrodes and devices by adhesion lithography, Nat. Commun. 27 May 2014 (Accessed 13 February 2017); 5, http://nature.com/doifinder/10.1038/ncomms4933

[45] Semple J, Rossbauer S and Anthopoulos T D 2016 Analysis of schottky contact formation in coplanar Au/ZnO/Al nanogap radio frequency diodes processed from solution at low temperature *ACS Appl. Mater. Interfaces* **8** 23167–74

[46] Semple J *et al* 2016 Radio frequency coplanar ZnO schottky nanodiodes processed from solution on plastic substrates *Small* **12** 1993–2000

[47] Lüssem B, Riede M and Leo K 2013 Doping of organic semiconductors *Phys. Status Solidi* a **210** 9–43

[48] Kleemann H, Schumann S, Jörges U, Ellinger F, Leo K and Lüssem B 2012 Organic pin-diodes approaching ultra-high-frequencies *Org. Electron.* **13** 1114–20

[49] Kleemann H *et al* 2010 Organic zener diodes: tunneling across the gap in organic semiconductor materials *Nano Lett.* **10** 4929–34

[50] Kleemann H, Gutierrez R, Avdoshenko S, Cuniberti G, Leo K and Lüssem B 2013 Reverse breakdown behavior in organic pin-diodes comprising C60 and pentacene: experiment and theory *Org. Electron.* **14** 193–9

[51] Krebs F C 2009 Fabrication and processing of polymer solar cells: a review of printing and coating techniques *Sol. Energy Mater. Sol. Cells* **93** 394–412

[52] Haldi A, Sharma A Jr, W J Potscavage Jr and Kippelen B 2008 Equivalent circuit model for organic single-layer diodes *J. Appl. Phys.* **104** 064503

[53] Steudel S *et al* 2005 50 MHz rectifier based on an organic diode *Nat. Mater.* **4** 597–600

[54] Lin C-Y *et al* 2011 High-frequency polymer diode rectifiers for flexible wireless power-transmission sheets *Org. Electron.* **12** 1777–82

[55] Yoon W-J, Chung S-Y, Berger P R and Asar S M 2005 Room-temperature negative differential resistance in polymer tunnel diodes using a thin oxide layer and demonstration of threshold logic *Appl. Phys. Lett.* **87** 203506

[56] Li M, Heljo P S and Lupo D 2012 Organic diodes for RF harvesting *Proc. LOPE-C (Munich)*

[57] Li M, Heljo P S and Lupo D 2014 Organic rectifying diode and circuit for wireless power harvesting at 13.56 MHz *IEEE Trans. Electron Devices* **61** 2164–9

[58] Lilja K E, Bäcklund T G, Lupo D, Hassinen T and Joutsenoja T 2009 Gravure printed organic rectifying diodes operating at high frequencies *Org. Electron.* **10** 1011–4

[59] Heljo P S, Li M, Lilja K E, Majumdar H S and Lupo D 2013 Printed half-wave and full-wave rectifier circuits based on organic diodes *IEEE Trans. Electron Devices* **60** 870–4

[60] Heljo P, Lilja K E, Majumdar H S and Lupo D 2014 High rectifier output voltages with printed organic charge pump circuit *Org. Electron.* **15** 306–10

[61] Heljo P S, Schmidt C, Klengel R, Majumdar H S and Lupo D 2015 Electrical and thermal analysis of frequency dependent filamentary switching in printed rectifying diodes *Org. Electron.* **20** 69–75

[62] Pal B N, Sun J, Jung B J, Choi E, Andreou A G and Katz H E 2008 Pentacene-zinc oxide vertical diode with compatible grains and 15 MHz rectification *Adv. Mater.* **20** 1023–8

[63] Sun J, Pal B, Jung B and Katz H 2009 Solution-processed hybrid p–n junction vertical diode *Org. Electron.* **10** 1–7

[64] Labram J G *et al* 2015 Signatures of quantized energy states in solution-processed ultrathin layers of metal-oxide semiconductors and their devices *Adv. Funct. Mater.* **25** 1727–36

[65] Sani N *et al* 2014 All-printed diode operating at 1.6 GHz *Proc. Natl Acad. Sci.* **111** 11943–8

[66] Brabec C J (ed) 2003 *Organic Photovoltaics: Concepts and Realization* (*Springer Series in Materials Science*) (New York: Springer) p 297

[67] Lin Y-H *et al* 2011 High-efficiency inverted polymer solar cells with solution-processed metal oxides *Sol. Energy Mater. Sol. Cells* **95** 2511–5

[68] Oh H, Krantz J, Litzov I, Stubhan T, Pinna L and Brabec C J 2011 Comparison of various sol–gel derived metal oxide layers for inverted organic solar cells *Sol. Energy Mater. Sol. Cells* **95** 2194–9

[69] You J *et al* 2012 Metal oxide nanoparticles as an electron-transport layer in high-performance and stable inverted polymer solar cells *Adv. Mater.* **24** 5267–72

[70] Huang H-C and Hsieh T-E 2010 Highly stable precursor solution containing ZnO nanoparticles for the preparation of ZnO thin film transistors *Nanotechnology* **21** 295707

[71] White M S, Olson D C, Shaheen S E, Kopidakis N and Ginley D S 2006 Inverted bulk-heterojunction organic photovoltaic device using a solution-derived ZnO underlayer *Appl. Phys. Lett.* **89** 143517

[72] Ho P-Y *et al* 2013 The effects of $MoO_3$ treatment on inverted PBDTTT-C:PC71BM solar cells *Sol. Energy Mater. Sol. Cells* **119** 235–40

[73] Chen L, Xie C and Chen Y 2014 Optimization of the power conversion efficiency of room temperature-fabricated polymer solar cells utilizing solution processed tungsten oxide and conjugated polyelectrolyte as electrode interlayer *Adv. Funct. Mater.* **24** 3986–95

[74] Ai Y *et al* 2007 14 MHz organic diodes fabricated using photolithographic processes *Appl. Phys. Lett.* **90** 262105

[75] Myny K, Steudel S, Vicca P, Genoe J and Heremans P 2008 An integrated double half-wave organic Schottky diode rectifier on foil operating at 13.56 MHz *Appl. Phys. Lett.* **93** 093305

[76] Products NFC Solutions, Thinfilm, (Accessed 27 April 2017), http://thinfilm.no/products-nfc-solutions/

[77] Lehtimäki S *et al* 2014 Performance of printable supercapacitors in an RF energy harvesting circuit *Int. J. Electr. Power Energy Syst.* **58** 42–6

[78] Steudel S, Myny K, Vicca P, Cheyns D, Genoe J and Heremans P 2008 Ultra-high frequency rectification using organic diodes *IEEE Int. Elect. Devices Meeting* **2008** 1–4

[79] Sani N *et al* 2016 Flexible lamination-fabricated ultra-high frequency diodes based on self-supporting semiconducting composite film of silicon micro-particles and nano-fibrillated cellulose *Sci. Rep.* **6** 28921

[80] Georgiadou D G, Semple J and Anthopoulos T D Adhesion lithography for fabrication of printed radio-frequency diodes, SPIE Newsroom, 16 January 2017 (Accessed 20 March 2017), http://spie.org/x124405.xml

[81] Mutlu S, Haydaroglu I and Sevim A O 2011 Realization of polymer charge pump circuits using polymer semiconductors *Org. Electron.* **12** 312–21

[82] Heljo P, Lilja K E, Tuukkanen S and Lupo D 2011 Charge pump circuit using printed organic diodes and capacitors *Proc. LOPE-C* pp 53–5

[83] Park H, Kang H, Lee Y, Park Y, Noh J and Cho G 2012 Fully roll-to-roll gravure printed rectenna on plastic foils for wireless power transmission at 13.56 MHz *Nanotechnology* **23** 344006

[84] Jung M *et al* 2010 All-printed and roll-to-roll-printable 13.56 MHz-operated 1-bit RF tag on plastic foils *IEEE Trans. Electron. Devices* **57** 571–80

[85] Ng T N *et al* 2016 Pulsed voltage multiplier based on printed organic devices *Flex Print Electron.* **1** 015002

[86] Takahashi K *et al* 1991 A high image-quality LCD addressed by lateral MIM *Conf. Record of the 1991 Int. Display Research Conf.* pp 247–50

[87] Muir S, Meyer J and Brewer J Amorphous-metal thin films enable ultra-high-definition display backplanes, SID Information Display, (Accessed 20 March 2017), http://informationdisplay.org/IDArchive/2016/JanuaryFebruary/FrontlineTechnologyAmorphousMetal.aspx

[88] Lilja K E, Bäcklund T G, Lupo D, Virtanen J, Hämäläinen E and Joutsenoja T 2010 Printed organic diode backplane for matrix addressing an electrophoretic display *Thin Solid Films* **518** 4385–9

[89] Virtanen J and Lupo D Active-matrix electronic display comprising diode based matrix driving circuit, US8395611 B2, 2013 (Accessed 6 March 2017), http://google.com/patents/US8395611

[90] Esaki L 1958 New phenomenon in narrow germanium p–n junctions *Phys. Rev.* **109** 603–4

[91] van der Wagt J P A 1999 Tunneling-based SRAM *Proc. IEEE* **87** 571–95

[92] van der Wagt J P A, Seabaugh A and Beam E RTD/HFET low standby power SRAM gain cell, in IEEE; 1996 (Accessed 8 February 2017), pp 425–8, http://ieeexplore.ieee.org/document/553618/

[93] Anisha R, Park S-Y and Berger P R 2011 90 nm 32 × 32 bit tunneling SRAM memory array with 0.5 ns write access time, 1 ns read access time and 0.5 Volt operation *IEEE Trans. Circuits Syst.* I **58** 2432–45

[94] Maezawa K, Akeyoshi T and Mizutani T 1994 Functions and applications of monostable-bistable transition logic elements (MOBILE's) having multiple-input terminals *IEEE Trans. Electron. Devices* **41** 148–54

[95] Cidronali A *et al* 2002 Ultralow DC power VCO based on InP-HEMT and heterojunction interband tunnel diode for wireless applications *IEEE Trans. Microw. Theory Tech.* **50** 2938–46

[96] Sollner T C L G, Goodhue W D, Tannenwald P E, Parker C D and Peck D D 1983 Resonant tunneling through quantum wells at frequencies up to 2.5 THz *Appl. Phys. Lett.* **43** 588–90

[97] Berger P R and Anisha R 2011 Negative differential resistance devices and circuits *Comprehensive Semiconductor Science and Technology* (Amsterdam: Elsevier) pp 176–241

[98] Chen J, Reed M A, Rawlett A M and Tour J M 1999 Large on-off ratios and negative differential resistance in a molecular electronic device *Science* **286** 1550–2

[99] Eppler A M, Ballard I M and Nelson J 2002 Charge transport in porous nanocrystalline titanium dioxide *Physica* E **14** 197–202

[100] Strukov D B, Snider G S, Stewart D R and Williams R S 2008 The missing memristor found *Nature* **453** 80–3

[101] Williams R 2008 How we found the missing memristor *IEEE Spectr.* **45** 28–35

[102] Tsu R and Esaki L 1973 Tunneling in a finite superlattice *Appl. Phys. Lett.* **22** 562–4

[103] Chang L L, Esaki L and Tsu R 1974 Resonant tunneling in semiconductor double barriers *Appl. Phys. Lett.* **24** 593–5

[104] Heljo P S *et al* 2014 Anodic oxidation of ultra-thin Ti layers on ITO substrates and their application in organic electronic memory elements *Electrochim. Acta* **137** 91–8

[105] Guttman J, Chambers C, Heinonen P, Lupo D and Berger P R 2015 Fabrication and defect properties of ultra-thin $TiO_2$ interfacial layers for hybrid tunnel diodes *MRS Fall Meeting (Boston, MA)*

[106] Guttman J J, Chambers C B, Villagracia A R, Santos G N C and Berger P R 2017 Negative differential resistance in polymer tunnel diodes using atomic layer deposited, $TiO_2$ tunneling barriers at various deposition temperatures *Org. Electron.* **47** 228–34

[107] Heinonen P P Fabrication of organic tunnel diodes with ultra-thin $TiO_2$ interfacial layers [Tampere]: Tampere University of Technology; 2015 (Accessed 8 February 2017), http://dspace.cc.tut.fi/dpub/handle/123456789/23058